Defence Research and Development Canada
Recherche et développement pour la défense Canada

The Concentration Probability Density Function With Implications for Probabilistic Modeling of Chemical Warfare Agent Detector Responses for Source Reconstruction

E. Yee

Defence R&D Canada

Technical Report

DRDC Suffield TR 2008-077

May 2008

Canada

The Concentration Probability Density Function With Implications for Probabilistic Modeling of Chemical Warfare Agent Detector Responses for Source Reconstruction

E. Yee
Defence R&D Canada – Suffield

Defence R&D Canada – Suffield

Technical Report

DRDC Suffield TR 2008-077

May 2008

Principal Author

Original signed by E. Yee

E. Yee

Approved by

Original signed by Mr C. Laforce

Mr C. Laforce
Head, Personal Protection Sector

Approved for release by

Original signed by Dr P. D'Agostino

Dr P. D'Agostino
Chair, DRDC Suffield DRP

Abstract

The relationships between various normalized higher-order concentration moments have been investigated using a large data set of concentration fluctuations obtained in a boundary-layer water channel with high-resolution laser-induced fluorescence. This data set corresponds to a series of comprehensive measurements of plume dispersion in a number of obstacle arrays (e.g., various arrays of cubical and non-cubical obstacles in aligned and staggered arrangements with uniform and random heights). A remarkably robust feature of all the concentration data was the observed collapse, of the third- and fourth-order normalized concentration moments on the second-order normalized concentration moment and of the concentration kurtosis on the concentration skewness, to a series of "universal" curves. These "universal" curves were identical to those observed previously for open-terrain plumes, and are well modeled using either a clipped-gamma probability density function (PDF) or the simpler intermittent exponential PDF for the concentration. A comparison of the shape of the model probability distributions to the measured concentration data at various plume locations showed that the clipped-gamma distribution provided a good representation for the general distribution shape, whereas the simpler intermittent exponential distribution yielded a poor conformance to the measured concentration probability distribution (in spite of the fact that both of the model distributions gave a good representation for the first four concentration moments). The implication of the form of the concentration PDF, for the formulation of a probabilistic model for the response of a chemical agent detector, is investigated in the context of the source reconstruction problem.

Résumé

On a étudié les relations entre des moments variés de concentrations d'ordre élevé normalisées en utilisant un ensemble important de données de fluctuations de concentrations obtenues par fluorescence induite au laser de haute résolution dans une voie d'eau à couche limite. Cet ensemble de données correspond à une série de mesures compréhensives de dispersions en panaches dans un certain nombre de réseaux d'obstacles (ex. : des réseaux variés d'obstacles cubiques et non cubiques, arrangés en lignes ou décalés et de hauteurs uniformes ou aléatoires). On a observé une caractéristique remarquablement robuste de toutes les données de concentrations, consistant en l'affaissement observé des moments de concentrations normalisées de troisième et quatrième ordre sur le moment de concentration normalisée de deuxième ordre et de l'aplatissement de la concentration sur l'étalement de la concentration, en une série de courbes " universelles ". Ces courbes " universelles " étaient identiques à celles observées auparavant pour des panaches en terrains ouverts et elles sont bien modélisées en utilisant soit une densité de probabilité gamma partielle soit une densité de probabilité exponentielle intermittente plus simple de la concentration. On a comparé la forme des distributions de probabilités du modèle avec les données de la concentration mesurée en des endroits variés du panache et on a trouvé que la distribution gamma partielle procurait une bonne représentation de la forme générale de la distribution alors que la distribution exponentielle intermittente plus simple se conformait peu à la distribution de probabilités de la concentration mesurée (en dépit du fait que les deux modèles de distribution donnaient une bonne représentation des quatre premiers moments de concentrations). On étudie actuellement quelles sont les implications de la forme de la densité de probabilité de la concentration dans la formulation du modéle probabiliste concernant la réponse du détecteur d'agents chimiques, dans le contexte du problème de la reconstruction de source.

Executive summary

The Concentration Probability Density Function With Implications for Probabilistic Modeling of Chemical Warfare Agent Detector Responses for Source Reconstruction

E. Yee; DRDC Suffield TR 2008-077; Defence R&D Canada – Suffield; May 2008.

Background: A critical capability gap in current emergency and retrospective management efforts directed at terrorist incidents involving the covert release of chemical, biological and radiological (CBR) agents into the atmosphere, is the determination of the number of sources and for each of these sources the location, amount of agent released, and time of release following event detection by a network of CBR sensors. In order to address this capability gap, a multi-national collaborative program for the development of methodologies for source reconstruction, involving the fusion of CBR concentration measurements from remote and deployable networks of sensors with model concentration data obtained from advanced atmospheric dispersion models, has been included as a task under The Technical Cooperation Program (TTCP), CBR Group Technical Panel 9 on Hazard Assessment.

Principal results: A probabilistic model for the response of a chemical agent detector, that provides concentration measurements in the form of a finite number of discrete bar levels, is formulated. This requires that the probability law governing the instantaneous concentration in hazardous plumes dispersing over level, unobstructed terrain and built-up (urban) terrain be known. Towards this purpose, a simple probability model for the plume concentration has be formulated and validated using a large data set of measurements of plume dispersion in idealized obstacle arrays. This data set was obtained from a comprehensive laboratary study in a water channel facility.

Significance of results: Many operational chemical agent detectors provide only measurements of concentration at a finite number of discrete levels or bars (such as, for example, the Chemical Agent Monitor (CAM) developed by Smiths Detection or the AP4C vapor detector developed by Proengin Inc.). The probabilistic model for a bar-level chemical agent detector developed in this report can be used directly in source reconstruction methodologies that have been developed previously to determine unknown source characteristics (e.g., location, source strength, time of release, etc.) when given a finite number of noisy and continuous level concentration measurements made by an array of detectors. With this development, the sensor-driven modeling paradigm can be integrated into operational warning and reporting (information) systems that combine automated data acquisition, analysis, source reconstruction, display, and distribution of CBR hazard prediction and decision-support products. This will lead to a more complete situational awareness in current warning and reporting systems for the operational CBR environment.

Future work: Future plans will include incorporating the proposed probabilistic model for chemical agent bar-level detectors into source reconstruction algorithms. This will provide a methodology for the fusion of operational chemical agent detector data (e.g., such as those obtained from in-service CAM or AP4C detectors) with model predictions of chemical agent dispersal in the atmosphere.

Sommaire

The Concentration Probability Density Function With Implications for Probabilistic Modeling of Chemical Warfare Agent Detector Responses for Source Reconstruction

E. Yee ; DRDC Suffield TR 2008-077 ; R & D pour la défense Canada – Suffield ; mai 2008.

Contexte : Il existe une lacune importante en termes de capacités en efforts de gestion rétroactive des situations d'urgence actuelles comportant l'mission cachée d'agents chimiques, biologiques et radiologiques (CBR) dans l'atmosphère puisqu'il faudrait être capable de déterminer le nombre de sources, et pour chacune de ces sources, le lieu d'émission, la quantité d'agent émis et l'heure de l'émission détectée par un réseau de capteurs CBR. Pour être en mesure de combler cette lacune, le Programme de Coopération technique, Panel 9 du Groupe technique CBR d'évaluation des dangers comporte une nouvelle tâche. Cette tâche consiste en un programme multinational concerté de développement des méthodologies de reconstruction de sources, comprenant notamment la fusion des mesures des concentrations CBR provenant de réseaux de capteurs éloignés pouvant être déployés et ayant des données de modèles de concentrations obtenues par des modèles perfectionnés de dispersion atmosphérique.

Résultats principaux : On a formulé un modéle probabiliste d'intervention consistant en un détecteur d'agent chimique qui fournit les mesures de concentration sous forme d'un nombre fini de niveaux de barres discrets. Ceci exige de connaître les lois de probabilité qui gouvernent les concentrations instantanées de panaches dangereux se dispersant sur un terrain nivelé, non obstrué et construit (urbain). À cette fin, on a formulé et validé un modèle simple de probabilités de la concentration des panaches, en utilisant un ensemble important de données des mesures de la dispersion du panache, dans des échantillons idéalisés d'obstacles. On a obtenu cet ensemble de donées au moyen d'une étude compréhensive dans une installation de voie d'eau en laboratoire.

Portée des résultats : Beaucoup de détecteurs d'agents chimiques opérationnels ne fournissent que les mesures de concentration à un nombre fini de niveaux ou de barres discrets (tels que par exemple le moniteur d'agents chimiques - CAM - mis au point par Smiths Detection ou le détecteur de vapeurs AP4C mis au point par Proengin Inc.). Le modèle probabiliste de détecteur d'agents chimiques, mis au point dans ce rapport, peut être directement utilisé dans les méthodologies de reconstruction des sources développées auparavant pour déterminer les caractéristiques des sources inconnues (ex. : lieu, puissance des sources, heure d'émission, etc.), ceci étant donné un nombre fini des mesures des niveaux de concentration bruyants et continus effectuées par un réseau de détecteurs. Cette mise au point permet d'intégrer le paradigme de modélisation à base de capteurs dans des systèmes opérationnels de signal d'avertissement et de transmission de données (informations) qui combine les données d'acquisition informatisées, les analyses, les sources de reconstruction,

d'affichage et de distribution de la prédiction des dangers CBR et des produits de soutien de prise de décision. Ceci amènera à une connaissance plus complète de la situation de l'environnement opérationnel CBR provenant des systèmes actuels d'avertissements et de transmission de données.

Perspectives d'avenir : On prévoit d'inclure, dans les algorithmes de reconstruction de sources, l'incorporation de ce modèle probabiliste, proposé ici, aux détecteurs à barres de niveaux d'agents chimiques. Ceci devrait fournir une méthodologie permettant de fusionner les données opérationnelles des détecteurs d'agents chimiques (comme par exemple celles obtenues du service interne de détecteurs CAM ou AP4C) avec le modèle de prédiction de la dispersion d'agents chimiques dans l'atmosphère.

Table of contents

List of figures

List of symbols and nomenclature

b_i	i-th bar level (provided by chemical agent detector)
C	ensemble-mean concentration
C_p	ensemble-mean concentration predicted by dispersion model
c	possible sample space values assumed by instantaneous concentration
$c_i^<$	lower concentration bound defining i-th bar level
$c_i^>$	upper concentration bound defining i-th bar level
c_m	measured concentration value
$\overline{c^2}$	mean-squared concentration ($\equiv \langle \chi^2 \rangle$)
$\overline{c^2}_p$	mean-square concentration predicted by dispersion model
$\overline{c'^2}$	concentration variance ($\equiv \overline{c^2} - C^2$)
$\overline{c'^2}\|_{\tau_a}$	concentration variance perceived by a detector with averaging time τ_a
d	zero-plane displacement
$\mathrm{erf}(x)$	error function
$F(c)$	cumulative distribution function for concentration
$f(c)$	probability density function for concentration
$f(c_m\|c)$	probability density function for measured concentration
$f(C\|S)$	probability density function for C given source distribution S
$f(\overline{c^2}\|S)$	probability density function for $\overline{c^2}$ given source distribution S
$H(x)$	Heaviside unit step function
k, s, λ	parameters defining clipped-gamma distribution
k_v	von Karman's constant (≈ 0.4)
$\mathcal{L}(b_i\|S)$	likelihood that detector reports bar level b_i for given source distribution S
N_b	number of bar levels provided by a chemical agent detector
$p(b_i)$	probability for detector to report bar level b_i
T_c	integral time scale for concentration fluctuations
u_*	friction velocity ($\equiv (-\overline{u'w'})^{1/2}$)
$\overline{u'w'}$	Reynolds shear stress
z_0	roughness length
$\Gamma(x)$	gamma function
$\Gamma(\nu; x)$	complementary incomplete gamma function
γ	intermittency factor (probability of observing a non-zero concentration χ)
$\delta(x)$	Dirac delta function
λ_f	frontal area index
λ_p	plan area index
σ_1	measurement noise standard deviation for concentration
σ_2	standard deviation (uncertainty) in prediction of mean concentration, C_p
σ_3	standard deviation (uncertainty) in prediction of mean-square concentration, $\overline{c^2}_p$
τ_a	averaging time imposed by chemical agent detector
χ	instantaneous (random) concentration
$\langle \cdot \rangle$	ensemble-averaging operation

This page intentionally left blank.

1 Introduction

The concentration in clouds and plumes of noxious pollutants (e.g., chemical and biological warfare agents) is inherently a random variable, owing to the stochastic nature of the turbulent processes responsible for dispersion in the atmosphere. The often neglected problem of concentration fluctuations in turbulent diffusion has received increasing interest over the past 25 years, owing to the fact that a knowledge of the characteristics of concentration fluctuations is of considerable importance in many industrial and environmental fluid mechanics problems. For example, the statistical properties of concentration fluctuations in a dispersing plume are important to the assessment of risk from the release of certain highly toxic materials (e.g., industrial chemicals, chemical warfare agents) in which there is a nonlinear relationship between concentration and duration of exposure for a given level of harmful effect [1], [2]. Similarly, short-term concentration fluctuations are very relevant to estimating ignition hazard from the leakage of flammable gases (e.g., fuel-air mixtures, liquified natural gas spills) in which it is necessary to determine the probability that the instantaneous concentration lies between the lower and upper flammability limits [3]. Still other important applications include the prediction of the probability of visibility through obscurant clouds, the characterization of the perception of odours required to evaluate the nuisance due to malodourous substances, and the understanding of fast nonlinear physiochemical processes required for the design of efficient mixing and combustion processes [4].

The statistical description of the natural random fluctuations in the instantaneous concentration of a plume dispersing in the atmosphere is conveniently embodied in the probability density function (PDF) of concentration. More specifically, in order to investigate and model concentration fluctuation phenomenology, it is useful to know the probability density function of concentration which necessarily embodies all the higher-order concentration moments of the stochastic process. Chatwin [5] discusses the importance of the concentration probability density function with reference to the assessment of hazards posed by the release of flammable and toxic gases. In particular, he emphasizes the need to characterize precisely the upper tail of the probability density function in order to determine exceedances of critical threshold levels by peak concentrations.

The shape and form of the concentration PDF of dispersing clouds and plumes of contaminant in the atmosphere have been studied by numerous investigators. In consequence, a number of models have been proposed for the concentration PDF. The lognormal distribution for concentration was proposed by Csanady [6] and used by Jones [7]. The exponential distribution was advocated by Barry [8] and applied by Hanna [9]. The clipped-normal distribution was proposed by Lewellen and Sykes [10] through application of the principle of maximum entropy and adopted by Sawford [11] and Mylne and Mason [12] as the distribution that best represents the concentration fluctuation data. Yee et al [13] tested seven candidate probability distributions including the gamma, Weibull, and conjugate beta distributions with reference to concentration fluctuation measurements obtained in a water channel. Finally, Yee and Chan [14] proposed a clipped-gamma distribution for the concentration PDF and demonstrated that this distribution provided excellent agree-

ment with the observed higher-order concentration moment relationships obtained from high-resolution concentration fluctuation measurements made during the cooperative Concentration Fluctuation Experiments (CONFLUX) project [15], [16].

All the research effort cited above for the modeling of the underlying distributional shape of the fluctuating concentration focussed exclusively on plumes dispersing over level, unobstructed terrain. However, it needs to be emphasized that as the fraction of the World's population that lives in cities continues to grow, it is becoming increasingly important to address the urgent problem of modeling the dispersion of toxic materials in the urban environment. This modeling is challenging because it is necessarily characterized by the wide spectrum of length and time scales associated with the interaction of the wind flow with the complex geometries and interfaces (building configurations, network of streets) that comprise the urban fabric. Presently, there is a paucity of information concerning the statistical description of concentration fluctuations in plumes dispersing in urban (built-up) areas and, more particularly, the characterization of the shape of the one-point concentration PDF for instantaneous plumes dispersing within urban areas.

Nevertheless, a small number of studies have focussed on the elucidation of the statistical characteristics of concentration fluctuations in plumes dispersing in an urban environment. For example, Yee and Biltoft [17] extracted a number of concentration statistics (e.g., concentration variance, concentration PDF, various concentration time and length scales of dominant plume motions) in a plume dispersing through a large array of building-like obstacles. Gailis and Hill [18] reported a wide range of concentration statistics and other quantitative descriptors of plume behaviour for tracer dispersion within a large array of obstacles in a boundary-layer wind-tunnel simulation. Yee et al [19] provided detailed comparisons of concentration statistics in a plume dispersing through a large array of building-like obstacles at three different scales; namely, at full-scale in a field experiment, at 1:50 scale in a wind-tunnel simulation, and at 1:205 scale in a water-channel simulation. Finally, Klein et al [20] analyzed and compared concentration fluctuation measurements from the Joint Urban 2003 (JU2003) full-scale and wind-tunnel experiments.

The objective of this paper is to investigate how the structure of the statistical properties of a plume dispersing through regular arrays of obstacles, as manifested through the higher-order moments of concentration, are modified in comparison to those observed for a plume dispersing over a level, unobstructed terrain. The measured relationships between the various concentration moments for the array plumes will be compared with predictions of these relationships obtained from some simple models for the probability density function of concentration fluctuations. The utility of these simple probability distribution models to characterize the shape of the measured concentration probability distribution for an array plume is assessed. The implication of the form of the concentration PDF for the formulation of a probabilistic model for the response of a chemical agent detector, that provides concentration measurements only at a number of discrete levels or bars, is investigated in the context of the source reconstruction problem.

2 Models for concentration PDF

For a fixed point in space $\mathbf{x}$ and a given instant in time t, the random concentration field $\chi(\mathbf{x},t) > 0$ of a hazardous pollutant dispersing in the atmosphere, can be characterized by the one-point concentration PDF $f(c;\mathbf{x},t)$ defined by

$$f(c;\mathbf{x},t)dc \equiv \Pr\big\{c \le \chi(\mathbf{x},t) < c+dc\big\}. \tag{1}$$

Here, the right-hand side denotes the probability that the random variable $\chi(\mathbf{x},t)$ falls in the interval of sample space values between c and $c+dc$ for different realizations of the turbulent dispersion of the hazardous cloud or plume. In Yee and Chan [14], a new concentration PDF model corresponding to a left-shifted and clipped-gamma distribution, was proposed. In this model, the concentration PDF has the form

$$f(c;\mathbf{x},t) = \left(\frac{c+\lambda}{s}\right)^{k-1} \frac{\exp\big(-(c+\lambda)/s\big)}{s\Gamma(k)} + (1-\gamma)\delta(c), \tag{2}$$

with $k = k(\mathbf{x},t) > 0$, $s = s(\mathbf{x},t) > 0$, $\lambda = \lambda(\mathbf{x},t) \ge 0$, $\gamma = \gamma(\mathbf{x},t) \in [0,1]$, $\Gamma(x)$ is the gamma function, $\delta(x)$ is the Dirac delta function and the range for c is $0 \le c < \infty$. The total PDF of concentration in Eq. (2) is composed of a mixed fluid part (first term on right-hand side of equation) that results from in-plume mixing of eddies that contain the scalar contaminant, and an unmixed ambient fluid part (second term on right-hand side of equation) that is produced by plume meandering producing intermittent periods of zero concentration for a fraction of time $(1-\gamma)$. Alternatively, $\gamma = \Pr\{\chi(\mathbf{x},t)\} > 0$ is the intermittency factor that determines the probability of observing a non-zero concentration χ at a point $(\mathbf{x},t)$ in space-time.

The concentration PDF in Eq. (2) is completely determined by four parameters: namely, γ, k, s and λ. However, for practical applications, we require a simple concentration PDF that predicts an arbitrary moment of the concentration given information on only the two lowest-order moments of concentration; namely, the mean concentration (first-order moment) and the mean-square concentration (second-order moment). In other words, we require a simple PDF form that can be specified with no more than two parameters, and yet is capable of fitting observed cloud or plume concentration data over a wide range of atmospheric conditions (various diabatic conditions) and terrain types (level, unobstructed terrain, urban terrain, etc.). This constraint arises from the fact that currently, the most advanced dispersion models have difficulty in predicting even the two lowest-order concentration moments with sufficient accuracy [21].

To provide a special form of the clipped-gamma distribution that is determined by two (rather than four) parameters, Yee and Chan [14] introduced two additional constraints. Firstly, it was assumed that γ can be uniquely determined as the area remaining under the gamma PDF curve for $c > 0$ after a left-shift of c by the amount λ, so

$$\begin{aligned} \gamma = \gamma(k,s,\lambda) &= \int_{\lambda}^{\infty} \left(\frac{c}{s}\right)^{k-1} \frac{\exp(-c/s)}{s\Gamma(k)}\, dc \\ &= \frac{\Gamma(k;\lambda/s)}{\Gamma(k)}, \end{aligned} \tag{3}$$

where $\Gamma(\nu;x)$ denotes the complementary incomplete gamma function. With this assumption, we have $\gamma \to 1^-$ (i.e., non-intermittent plume concentration) when $\lambda \to 0^+$ (i.e., no left-shift)[1]. Secondly, concentration data measured in the CONFLUX project [15], [16] was used to provide a simple relation between the normalized mean-square concentration and plume intermittency:

$$\langle (\chi/C)^2 \rangle = 3/\gamma, \tag{4}$$

where $\langle \cdot \rangle$ denotes the ensemble average (viz., average over a number of independent realizations of a process) and C is the ensemble-averaged concentration (viz., $C = \langle \chi \rangle$).

Note that with the parameterization for γ given by Eq. (4), the plume concentration is implicitly assumed to be non-intermittent (viz., $\gamma = 1$) for $\langle (\chi/C)^2 \rangle \in [1,3]^2$ because γ cannot exceed unity in value. For a non-intermittent plume concentration, the concentration PDF of Eq. (2) reduces to a simple gamma PDF as $\gamma = 1$ and $\lambda = 0$ (which occurs when $\langle (\chi/C)^2 \rangle \in [1,3]$); viz., the concentration PDF reduces to

$$f(c;\mathbf{x},t) = \left(\frac{c}{s}\right)^{k-1} \frac{\exp(-c/s)}{s\Gamma(k)}, \tag{5}$$

when $\langle (\chi/C)^2 \rangle \in [1,3]$. More succinctly, this special form of the clipped-gamma distribution is defined with γ determined as

$$\gamma = \min\left(1, \frac{3}{\langle (\chi/C)^2 \rangle}\right), \tag{6}$$

so that when $\langle (\chi/C)^2 \rangle \in [1,3]$, $\gamma \equiv 1$ and $\lambda = 0$; and, the clipped-gamma distribution simplifies to the simple gamma distribution in this case.

The n-th concentration moment of Eq. (2) is given by

$$\begin{aligned} \langle \chi^n \rangle &= \int_0^\infty c^n f(c;\mathbf{x},t)\, dc \\ &= \sum_{j=0}^{n} \binom{n}{j} (-\lambda)^j s^{n-j} \frac{\Gamma(n-j+k;\lambda/s)}{\Gamma(k)}, \quad n \in \mathbb{N}. \end{aligned} \tag{7}$$

With the constraints given by Eqs. (3) and (6), the model concentration PDF parameters k, s and λ in Eq. (2) can be obtained by solving the following system of transcendental equations:

$$\frac{1}{s} = \left(-\frac{\lambda}{s} + k\right)\gamma + \frac{1}{\Gamma(k)} \left(\frac{\lambda}{s}\right)^k \exp(-\lambda/s); \tag{8}$$

$$\left\langle \left(\frac{\chi}{C}\right)^2 \right\rangle = \frac{\big((\lambda/s)\gamma + (-\lambda/s + k + 1)/s\big)}{\big[(-\lambda/s + k)\gamma + (\lambda/s)^k \exp(-\lambda/s)/\Gamma(k)\big]^2}; \tag{9}$$

[1] Note that $x \to a^-$ and $x \to a^+$ denotes the approach to x to the limiting value a from the left (viz., from values of x smaller than a) and from the right (viz., from values of x larger than a), respectively.

[2] The concentration variance $\langle \chi'^2 \rangle = \langle \chi^2 \rangle - C^2 \geq 0$ ($\chi' \equiv \chi - C$), so $\langle \chi^2 \rangle \geq C^2$ or, equivalently, $\langle (\chi/C)^2 \rangle \geq 1$ is the lower bound for the normalized mean-square concentration.

and

$$\gamma = \min\left(1, 3\left\langle\left(\frac{\chi}{C}\right)^2\right\rangle^{-1}\right) = \frac{\Gamma(k;\lambda/s)}{\Gamma(k)}. \tag{10}$$

Thence, for a specified value of $\langle(\chi/C)^2\rangle$, Eqs. (9) and (10) can be solved for k and (λ/s),[3] and these values can be subsequently substituted into Eq. (8) to obtain s, after which the value of λ can be deduced. The solution of these equations for k, s and λ as a function of $\langle(\chi/C)^2\rangle$ is exhibited in Figure 1.

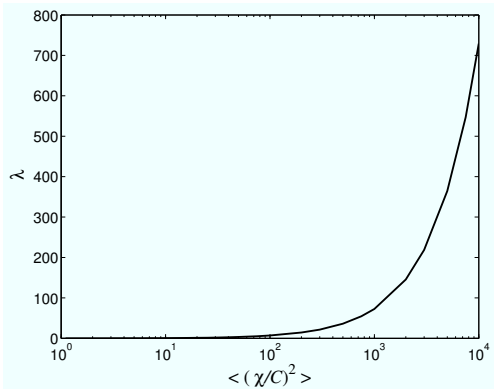

(a) Clipped-gamma parameter λ

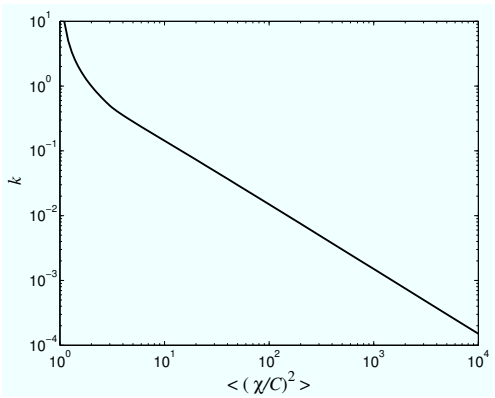

(b) Clipped-gamma parameter k

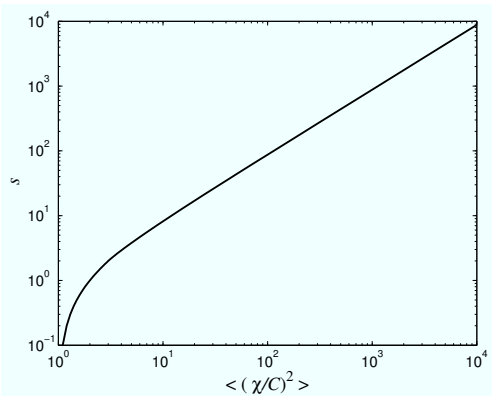

(c) Clipped-gamma parameter s

Figure 1: *Dependence of the parameters (k, s, and λ) of a clipped-gamma distribution on the normalized mean-square concentration $\langle(\chi/C)^2\rangle$.*

The skewness S and kurtosis K are defined by

$$S \equiv \frac{\langle\chi'^3\rangle}{\sigma_c^3} = \frac{\langle(\chi - C)^3\rangle}{\sigma_c^3}, \qquad K \equiv \frac{\langle\chi'^4\rangle}{\sigma_c^4} = \frac{\langle(\chi - C)^4\rangle}{\sigma_c^4}, \tag{11}$$

where $\sigma_c^2 \equiv \langle\chi'^2\rangle = \langle(\chi - C)^2\rangle$ is the variance of concentration. The skewness and kurtosis can be readily computed from the relationships between the central concentration moments

[3]Note that the factor $1/s$ in Eq. (9) can be expressed as a function of only k and (λ/s) using Eq. (8).

(moments about the mean concentration) and the concentration moments about the origin [cf. Eq. (7)]. It can be easily verified that the second-, third-, and fourth-order central concentration moments are related to the concentration moments about the origin as follows:

$$\sigma_c^2 \equiv \langle \chi'^2 \rangle = \langle \chi^2 \rangle - C^2, \tag{12}$$

$$\langle \chi'^3 \rangle = \langle \chi^3 \rangle - 3C\langle \chi^2 \rangle + 2C^3, \tag{13}$$

and

$$\langle \chi'^4 \rangle = \langle \chi^4 \rangle - 4C\langle \chi^3 \rangle + 6C^2\langle \chi^2 \rangle - 3C^4. \tag{14}$$

In view of the complexity of the clipped-gamma distribution of Eq. (2), it is useful to consider a simpler model for the concentration PDF; namely, the exponential PDF for intermittent concentrations proposed by Barry [8]. This concentration PDF is a two-parameter PDF that has the following simple form:

$$f(c;\mathbf{x},t) = \frac{\gamma^2}{C}\exp\left(-\frac{\gamma c}{C}\right) + (1-\gamma)\delta(c). \tag{15}$$

For this distribution, the intermittency factor is related to the normalized mean-square concentration as follows:

$$\gamma = \frac{2}{\langle (\chi/C)^2 \rangle}. \tag{16}$$

Furthermore, the relationship between the normalized higher-order and second-order concentration moments for the intermittent exponential PDF is given by

$$\left\langle \left(\frac{\chi}{C}\right)^n \right\rangle = \frac{\Gamma(n+1)}{2^{n-1}} \left\langle \left(\frac{\chi}{C}\right)^2 \right\rangle^{n-1}, \qquad n \in \mathbb{N}. \tag{17}$$

Strictly, the exponential PDF imposes the constraint that $\langle (\chi/C)^2 \rangle \geq 2$ [cf. Eq. (16)], owing to the fact that $\gamma \leq 1$. However, similar to the clipped-gamma distribution, we implicitly assume that $\gamma = 1$ when $\langle (\chi/C)^2 \rangle \in [1,2]$. In this case, the intermittent exponential PDF given by Eq. (15) reduces to the usual exponential PDF; viz.,

$$f(c;\mathbf{x},t) = \frac{1}{C}\exp\left(-\frac{c}{C}\right). \tag{18}$$

To summarize, γ for the intermittent exponential distribution is defined as

$$\gamma = \min\left(1, \frac{2}{\langle (\chi/C)^2 \rangle}\right), \tag{19}$$

so when $\langle (\chi/C)^2 \rangle \in [1,2]$, $\gamma = 1$ and the intermittent exponential distribution simplifies to the usual exponential distribution of Eq. (18).

It is interesting to note that the intermittent exponential distribution given by Eq. (15) can be considered to be a special case of the clipped-gamma distribution given by Eq. (2). In this form of the clipped-gamma distribution, Eq. (19) is used to relate the intermittency

factor to the normalized mean-square concentration, rather than the *ansatz* of Eq. (6). From Eq. (3), this immediately implies that

$$\gamma = \gamma(k, s, \lambda) = \min\left(1, 2\left\langle \left(\frac{\chi}{C}\right)^2 \right\rangle^{-1}\right) = \frac{\Gamma(k; \lambda/s)}{\Gamma(k)}. \tag{20}$$

Solving Eqs. (20) and (9) for k and λ/s, it can be shown that $k = 1$ and $\gamma = \exp(-\lambda/s)$, which by virtue of Eq. (8) implies that $s = 1/\gamma$. The latter value for s is appropriate for the normalized concentration χ/C (or equivalently, for a system of units where $C \equiv 1$). For the unnormalized concentration χ, $s = C/\gamma$. Using these values for k, γ and s in Eq. (2), the concentration PDF for this special case reduces to the form:

$$\begin{aligned} f(c; \mathbf{x}, t) &= \frac{1}{s}\exp\big(-(c/C + \lambda)/s\big) + (1-\gamma)\delta(c) \\ &= \frac{\gamma^2}{C}\exp\left(-\frac{\gamma c}{C}\right) + (1-\gamma)\delta(c), \end{aligned} \tag{21}$$

which is exactly the intermittent exponential PDF of Eq. (15).

3 Experimental data for model evaluation

Previously, a comprehensive concentration fluctuation data set obtained in field experiments during the September 1991, November 1992, May 1993, and May 1994 phases of the CONFLUX project was used for studying the relationships between the higher-order concentration moments [14] under a very wide range of atmospheric conditions. In this study, 1,107 individual CONFLUX concentration time series from a large number of different experiments covering a very wide range of atmospheric conditions were used. All these experiments involved the continuous and controlled release of propylene (C_3H_6) tracer gas into the atmosphere. The measurements were made at downwind fetches x of between 12.5 and 1,000 m from the source, under moderately convective to extremely stable atmospheric conditions in which mechanical turbulence was suppressed by the stable stratification. The concentration time series were measured over a wide range of receptor positions in both lateral and vertical cross-sections through the plume — lateral plume positions varied from the mean-plume centerline at $y/\sigma_y = 0$ to the extreme plume fringes at $y/\sigma_y \approx \pm 4$, where y is the crosswind distance from the mean-plume centerline and σ_y is the mean-plume dispersion; and, vertical positions ranged from 0.5 to 16 m height above ground. The source was placed at heights ranging from 1 to 5 m.

The analysis conducted by Yee and Chan [14], using this concentration fluctuation data set, showed that despite the diversity of the different field experiments which were undertaken under a wide range of atmospheric conditions, scatterplots of various higher-order normalized concentration moments $\langle(\chi/C)^n\rangle$ (n = 3, 4, 5, 6, 7, and 8) versus the second-order normalized concentration moment $\langle(\chi/C)^2\rangle$ each exhibited a remarkable collapse of the data onto a single curve. This collapse is a remarkably robust feature of the concentration data and provides compelling evidence that the concentration PDF can be represented (to a

very good approximation) with 2 parameters; namely, one for location (mean concentration) and one for scale (root mean-square concentration, or equivalently, concentration standard deviation). Furthermore, Yee and Chan [14] demonstrated that the clipped-gamma PDF provided good predictions of the observed relationships between various higher-order normalized concentration moments and the second-order normalized concentration moment.

This collapse of concentration data was demonstrated using measurements of plume dispersion over level, unobstructed terrain. In view of this, the question that we pose is as follows. Do the concentrations in a plume dispersing through and over an urban environment consisting of a large collection of buildings and other obstacles (e.g., cars lining a street, treed areas in city green spaces) exhibit a collapse of the higher-order concentration moments on the second-order concentration moment? If so, can this collapse be predicted using the clipped-gamma distribution as in the case of plume dispersion over level, unobstructed terrain?

To address these questions, we will use a large concentration data set obtained from measurements of the near-field dispersion of tracer plumes in different arrays of building-like obstacles. This comprehensive, high-quality data set of dispersion of array plumes was obtained from water channel simulations carried out at Coanda Research & Development Corporation's (Burnaby, British Columbia, Canada) boundary-layer water channel [22]. The water channel is specially designed for dispersion modeling and has a working section of 10 m length, 1.5 m width, and 0.9 m height. The upwind part of the working section of the water channel was used to generate a naturally grown neutrally-stratified rough-walled boundary layer of about 0.3 m thickness. This was accomplished using a "turbulence" grid made of square bars 19 mm $\times$ 19 mm placed at the start of the channel inlet to generate turbulence at the entry of the working section. A sawtooth fence with a base width equal to that of the channel and a height of 70 mm was placed 200 mm downstream of the square bar array. The combination of sawtooth fence and turbulence grid was used to trigger and produce some of the larger-scale eddies in the boundary layer.

Downstream of the sawtooth fence, the floor of the water channel was covered with a black anodized expanded metal mesh of height 4 mm with a total streamwise length of 6 m to give a sufficiently long fetch of uniform surface roughness for the upstream flow to develop. The expanded metal mesh had diamond-shaped holes that were approximately 11 mm long in the streamwise direction and 25 mm wide in the spanwise direction. After this uniform upstream fetch of expanded metal mesh, the flow then encountered the model obstacle array. Downstream of the obstacle array, the flow encountered a section covered with the same black anodized expanded metal mesh that was used for the initial upstream boundary-layer development.

Measurements of the vertical profiles of mean velocity, $\overline{u}$, streamwise velocity variance, $\sigma_u^2 \equiv \overline{u'^2}$, and shear stress $\tau \equiv \overline{u'w'}$ made using a 4-beam, 2-component fibre-optic laser Doppler velocimeter (LDV) within the equilibrium boundary layer upstream of the obstacle array, showed that these profiles were homogeneous to within $\pm 5\%$ in the spanwise direction across the channel.[4] The boundary-layer thickness, δ, taken to be the height where the mean

[4] Overbars and primes denote time averages and departures therefrom; and, (u, v, w) are the instantaneous

wind speed reached 99% of the free stream value, was found to be 275 mm. At this point, the mean wind speed $\overline{u}_\delta$ was 0.375 m s^{-1}. The friction velocity $u_* \equiv (-\overline{u'w'})^{1/2}$ determined from measurements of the shear stress in the constant stress layer near the surface was 0.0255 m s^{-1}, giving $u_*/\overline{u}_\delta = 0.068$ for the water channel simulations. A least-squares fit of the usual log-law profile for the mean wind speed in a regular rough-wall boundary layer, $\overline{u}/u_* = k_v \log\big[(z-d)/z_0\big]$, where z_0 is the roughness length, d is the zero-plane displacement, and $k_v \approx 0.4$ is von Karman's constant gave the following results: $z_0 = 0.35 \pm 0.05$ mm, assuming a zero-plane displacement d of 2.8 mm (using the common rule of thumb that d should be approximately 70% of the height of the roughness elements).

Six different types of obstacle arrays were used in this study. The first obstacle array is shown in Figure 2. This obstacle array corresponds to a 1:205 scale of a large array of building-like obstacles used for the Mock Urban Setting Test (MUST) field experiment conducted in September 2001 at U.S. Army Dugway Proving Ground [17]. For the water channel simulation of the MUST field experiment, each obstacle was a rectangular parallelipiped with a width of 59.4 mm, length of 11.8 mm, and height of 12.4 mm. A total of 120 obstacles was placed in an aligned configuration consisting of 12 rows of 10 obstacles with an obstacle spacing (face-to-face) of 38.5 mm in the spanwise (y) direction and 62.9 mm in the streamwise (x) direction (cf. Figure 2). The frontal (λ_f) and plan (λ_p) area indices of the obstacle array were 0.10 and 0.096, respectively.[5] The MUST obstacles for the water channel simulation were machined from anodized aluminum and installed on a lexan panel.

The remaining five obstacle arrays were composed of cubes and/or parallelipipeds (rectangular blocks), constructed from Lego$^{\text{TM}}$ blocks. These obstacle arrays were constructed from a square 'repeating' unit cell (63.5 mm $\times$ 63.5 mm) shown in Figure 3. The unit cell was divided into 4 quadrants labelled A, B, C, and D. Each obstacle (cube or rectangular block) of the array had a square cross section with a side length $H = 31.75$ mm. An obstacle can be placed on any one of these 4 quadrants in the unit cell. The obstacle arrays were constructed from a 16×16 unit cell array layout placed on a Lego$^{\text{TM}}$ baseplate.

Schematic drawings of the obstacle arrays constructed using cubes and/or parallelipipeds are shown in Figures 4 to 8. Each of these arrays had a plan area index $\lambda_p = 0.25$. For the arrays of aligned obstacles, the obstacles were placed in quadrant A of each unit cell of the array. For the array of staggered obstacles, the obstacles were placed in either quadrant A or C of each unit cell, in accordance to whether the obstacle row number (in the streamwise or flow direction) was even or odd, respectively.

The second obstacle array used in this study is shown in Figure 4 and corresponds to an aligned array of 31.75-mm cubes with a frontal area index of 0.25 (URB01). The third obstacle array, exhibited in Figure 5, consists of 31.75-mm cubes arranged in a regular staggered pattern with a frontal area index of 0.25 (URB02). The fourth obstacle array, displayed in Figure 6, is an aligned array of rectangular blocks with square cross-section of

velocities in the streamwise (x), spanwise (y) and vertical (z) directions, respectively.

[5] The frontal area index of an obstacle array is defined as $\lambda_f \equiv A_f/A_L$, where A_f is the frontal (windward) area of an obstacle and A_L is the lot area (surface area within which a single obstacle sits in the array). The plan area index is defined as $\lambda_p = A_p/A_L$, where A_p is the plan (floor) area of the obstacle.

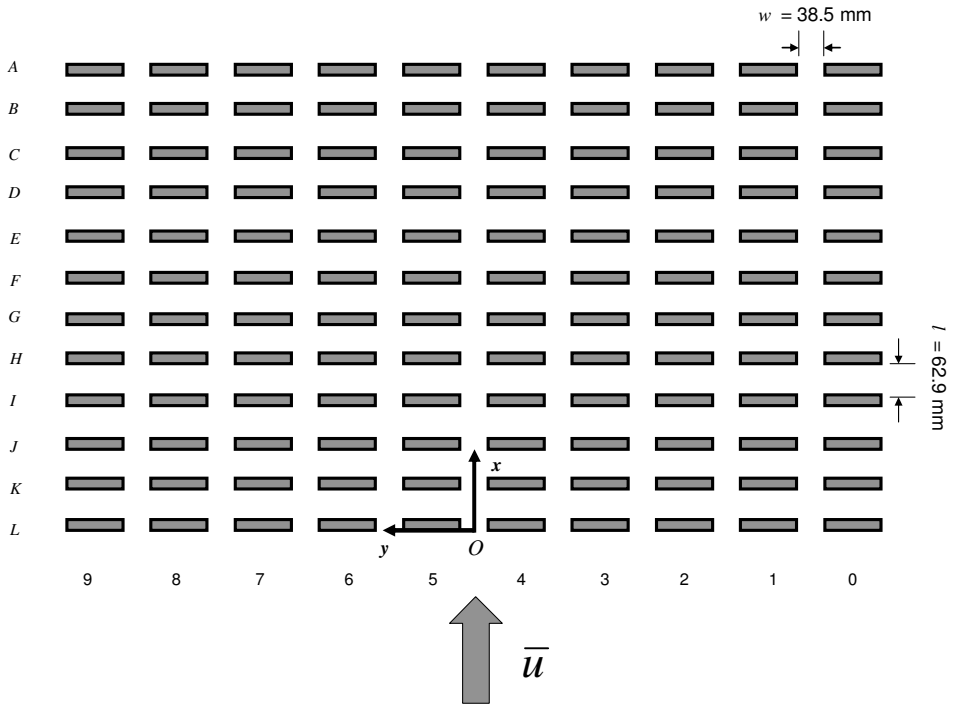

Figure 2: *A schematic diagram of the geometry of the Mock Urban Setting Test (MUST) obstacle array.*

side length H and height of $2H$ to give an array with a frontal area index of 0.5 (URB03). Figure 7 shows the fifth obstacle array used for this study, which corresponds to an aligned array of obstacles (cubes or rectangular blocks) with square cross-section H whose heights have been randomly chosen as H, $2H$, or $3H$ (URB04). Finally, the sixth obstacle array is shown in Figure 8, and consists of an aligned array of rectangular blocks with alternating rows of blocks having heights of $2H$ and $3H$ resulting in a frontal area index of 0.625 (URB10).

For the water channel simulations involving the six obstacle arrays summarized above, the point source consisted of a vertical stainless steel tube (2.8 mm I.D. and 3.1 mm O.D.). The source emitted a sodium fluorescein dye tracer at a constant flow rate of 12×10^{-3} l min^{-1} with low discharge momentum (weak vertical jet). For the MUST obstacle array, the point source was located at ground level at a position centered in the street canyon between obstacles $K4$ and $L4$ (cf. Figure 2). For arrays URB01 (Figure 4), URB02 (Figure 5), URB03 (Figure 6) and URB10 (Figure 8), the point source was located at ground level at two different positions: namely, at the center of quadrant D behind an obstacle in a spanwise-oriented street canyon and at the center of quadrant C between obstacles in a streamwise-oriented street canyon. These sources were located in the unit cell lying at the intersection of the first row and eighth column of obstacles (where the rows are numbered in increasing order in the streamwise direction from the leading (windward) edge of the array and the columns are numbered in increasing order in the spanwise direction from the

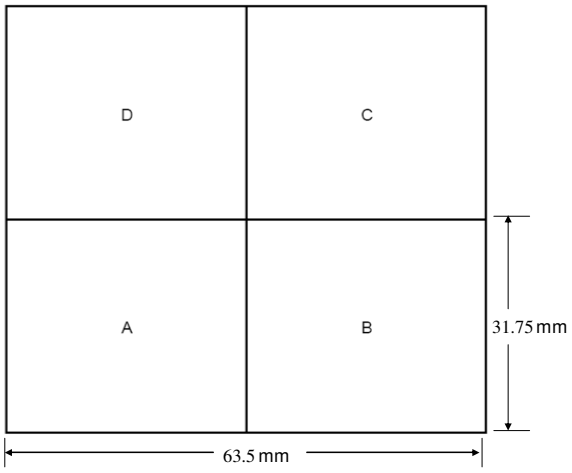

Figure 3: *Basic unit cell used to construct 'urban' obstacle arrays.*

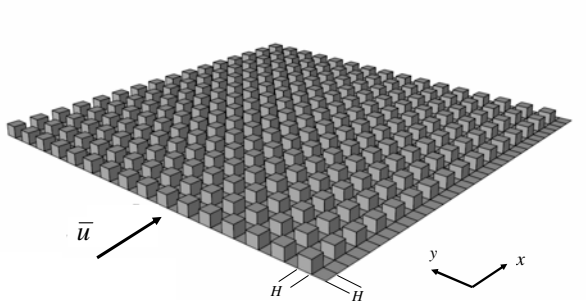

Figure 4: *Schematic of an aligned array of cubes of side length H with frontal area index $\lambda_f = 0.25$ and plan area index $\lambda_p = 0.25$ (URB01).*

right-hand side of the array when looking in the flow direction – see Figures 4 to 8). For array URB04 (Figure 7), the point source was located only at the center of quadrant D behind an obstacle in a spanwise-oriented street canyon.

The instantaneous concentration field in the dispersing dye plume was measured using the laser-induced fluorescence (LIF) technique, which permitted simultaneous multi-point concentration measurements to be acquired with very high spatial and temporal resolution. Here, the sodium fluorescein dye was illuminated with an argon-ion laser beam and the fluorescent intensities were measured with a digital monochrome charge-coupled device (CCD) camera with a 12-bit amplitude resolution. The LIF measurements of the concentration were carried out using a line-scan configuration with the line of laser light oriented in either

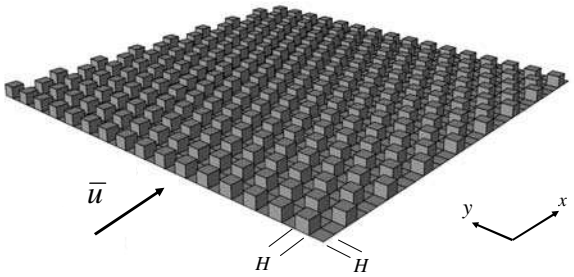

Figure 5: *Schematic of a staggered array of cubes of side length H with frontal area index $\lambda_f = 0.25$ and plan area index $\lambda_p = 0.25$ (URB02).*

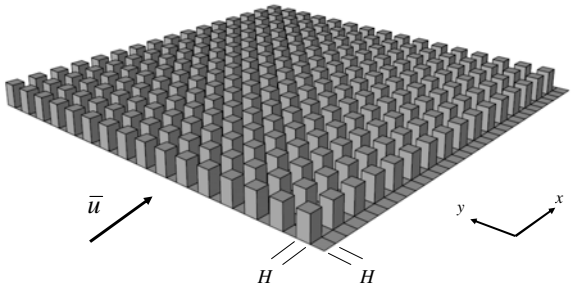

Figure 6: *Schematic of an aligned array of parallelepipeds, each having a square cross-section of side length H and a height of $2H$, with frontal area index $\lambda_f = 0.5$ and plan area index $\lambda_p = 0.25$ (URB03).*

a horizontal or vertical direction through the dispersing plume to provide a lateral or vertical profile of the instantaneous plume concentration at a fixed downstream distance from the source and at a fixed height above the ground surface. Each line scan consisted of 1,016 pixels in either a horizontal or vertical line across the channel, giving a spatial resolution between about 0.5 mm to 1 mm depending on the exact positioning of the camera and laser line. The line scans were sampled at 300 Hz. The sampling times for each experiment was 1,000 s, yielding $N = 300,000$ individual line scans per experiment. Each line scan LIF measurement provides an instantaneous realization of the plume concentration along the line of laser light, and the light intensity of each respective pixel along the line from an entire ensemble of N line scans can be averaged to obtain various concentration statistics (e.g., mean concentration, higher-order moments of concentration).

For all obstacle arrays except URB03, horizontal line scans through the dispersing array plume were made at a number of different downstream distances from the source, and for each of these downstream locations a number of vertical heights in the plume were sampled. For the MUST array (Figure 2), the horizontal line scans were made at five downstream

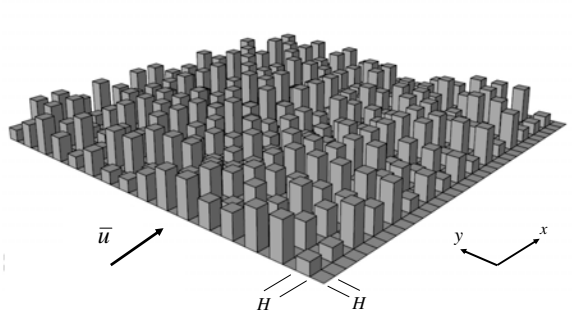

Figure 7: *Schematic of an aligned array of random-height parallelepipeds, each having a square cross-section of side length H and heights of either H, $2H$, or $3H$ chosen randomly, with plan area index $\lambda_p = 0.25$ (URB04).*

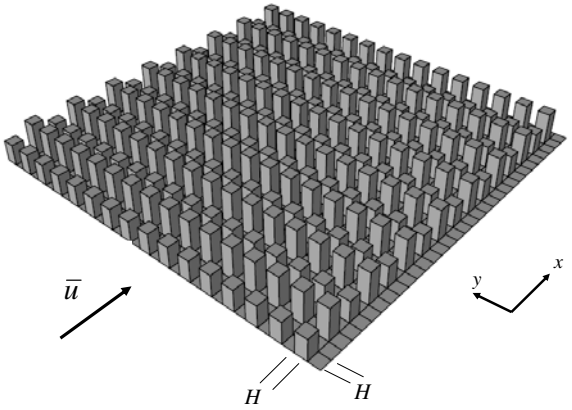

Figure 8: *Schematic of an aligned array of alternating-height parallelepipeds, each having a square cross-section of side length H and heights of $2H$ or $3H$ in alternating rows, with a frontal area index $\lambda_f = 0.625$ and plan area index $\lambda_p = 0.25$ (URB10).*

locations (i.e., rows 2.5, 3.5, 4.5, 6.5, and 9.5) and for each of these downstream positions at six different heights (i.e., at 0.5, 0.75, 1.0, 1.25, 1.5, and 2.0 times the obstacle height). Here, "row 2.5" refers to a streamwise location that is centered in the spanwise-oriented street canyon between rows 2 and 3 of the obstacle array, etc. For the URB01 and URB02 arrays (Figures 4 and 5), the horizontal line scans were made at six different downstream locations (rows 2.5, 3.5, 4.5, 6.5, 9.5, and 14.5) and for each of these locations at three different heights (i.e., at $z/H = 0.25$, 0.5 and 1.25). For array URB03, vertical line scans data were acquired for the dispersing plume along the mean plume centerline at six downstream distances from the source (rows 2.5, 3.5, 4.5, 6.5, 9.5, and 14.5). Finally, for arrays URB04 and URB10 (Figures 7 and 8), horizontal line scan data were acquired at four downstream distances from the source (rows 2.5, 3.5, 4.5, and 9.5) and at each of these locations for three different vertical heights (i.e., at $z/H = 0.5$, 1.25, and 3.25).

4 Concentration moments

The concentration time series, extracted from the measurements of plume dispersion through and over the six obstacle arrays described in the previous section, were processed to determine the normalized concentration moments up to order four (viz., we calculated $\langle(\chi/C)^n\rangle$ for $n = 2, 3, 4$ from the concentration data), as well as the skewness S and kurtosis K for the concentration.

Figure 9 displays double-logarithmic scatterplots (consisting of 8,359 data points) of the normalized third- and fourth-order concentration moments $\langle(\chi/C)^n\rangle$ $(n = 3, 4)$ against the normalized second-order concentration moment $\langle(\chi/C)^2\rangle$ and of kurtosis K against skewness S for the concentration data measured for the MUST obstacle array. Figures 10 and 11 exhibit the normalized concentration moment diagrams of $\langle(\chi/C)^n\rangle$ $(n = 3, 4)$ [consisting of 5,510 and 5,799 data points, respectively] plotted against $\langle(\chi/C)^2\rangle$ on a double-logarithmic scale and of K plotted against S for the aligned array of cubes (URB01) with the location of the ground-level source positioned in quadrants C and D, respectively. Similarly, Figures 12 and 13 present the results for the staggered array of cubes (URB02) for a ground-level source located in quadrants C and D consisting of 5,538 and 5,004 data points, respectively; and, Figures 14 and 15 show the normalized concentration moments diagrams for the aligned array of parallelepipeds of uniform height $2H$ for a ground-level source located in quadrants C and D consisting of 938 and 1,276 data points, respectively. Figure 16 presents scatterplots of the third- and fourth-order concentration moments versus the second-order concentration moment and of S versus K for the aligned array of random-height parallelepipeds (URB04) These plots consist of 2,749 concentration data points. Finally, Figures 17 and 18 exhibit the various normalized moment diagrams for concentration measurements in the aligned array of alternating-height parallelepipeds (URB10) with the ground-level source positioned in quadrants C and D consisting of 2,279 and 2,720 data points, respectively.

The points plotted in Figures 9–18 cover different types of obtacles arrays (e.g., cubical and non-cubical obstacles, different layouts of obstacles in the array, arrays with uniform, random, and alternating height obstacles, etc.) and a wide range of downwind, crosswind, and vertical plume positions both within and above the obstacle array. Even so, each of the scatterplots exhibited in Figures 9–18 seem to collapse onto a set of "universal" curves, suggesting that this collapse is a remarkably robust feature of the concentration data. This observed collapse suggests that there exist strong correlations between the various higher-order and second-order normalized concentration moments, the latter of which also implies the existence of a definitive relationship between the skewness S and kurtosis K of the concentration. It should be noted that there is more scatter in the plots of the normalized moment diagrams at the higher values of $\langle(\chi/C)^2\rangle$ (corresponding to positions in the plume that are closer to the plume edges) and at higher values of the moment order n. This increased scatter appears to be random, being most likely attributed to increased sampling errors arising from the measurement of concentration nearer the plume edges and/or of higher-order concentration moments.

The results of Figures 9–18 provide compelling evidence that the concentration PDF for

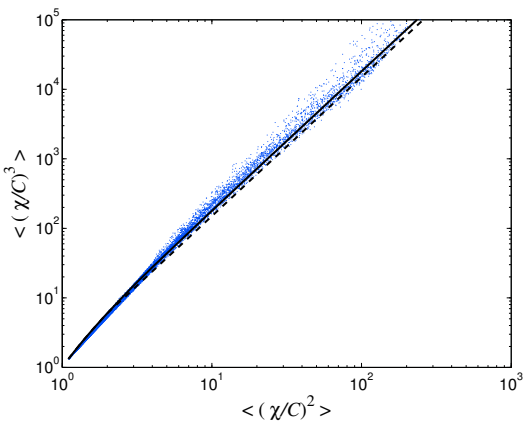

(a) $\langle(\chi/C)^2\rangle$ versus $\langle(\chi/C)^3\rangle$

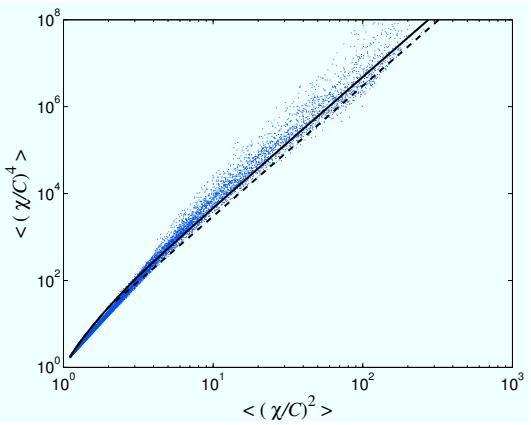

(b) $\langle(\chi/C)^2\rangle$ versus $\langle(\chi/C)^4\rangle$

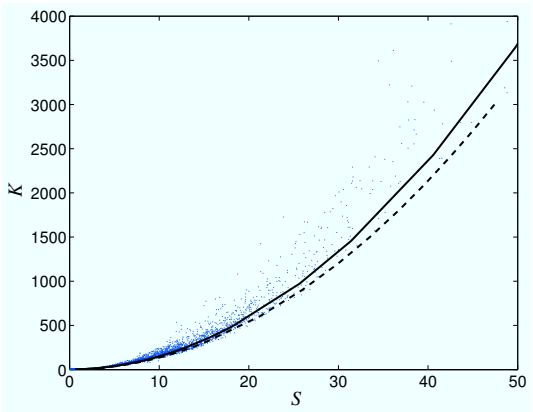

(c) S versus K

Figure 9: *Scattergrams of third- and fourth-order normalized concentration moments against the second-order normalized concentration moment and of skewness S against kurtosis K for the MUST obstacle array.*

a plume dispersing in a built-up environment (e.g., arrays of building-like obstacles) can be described by at most two parameters; namely, a location and a scale parameter for the PDF. This implies that one can use a simple two-parameter concentration PDF to predict (approximately or better) an arbitrary concentration moment given information on only the two lowest concentration moments [e.g., mean concentration and mean-square concentration (or, equivalently, concentration variance)]. As mentioned earlier, one of the goals was to investigate the higher-order concentration moment relationships for dispersing plumes in order to suggest an appropriate form for the concentration PDF that may be used to formulate a probabilistic model for the response of a chemical agent detector. Towards this objective, we consider two simple concentration PDF models (whose form is completely specified by two parameters) and examine their flexibility in representing the observed higher-order concentration moment relationships measured in a built-up environment; namely, the clipped-gamma and intermittent exponential PDFs [cf. Eqs. (2) and (15),

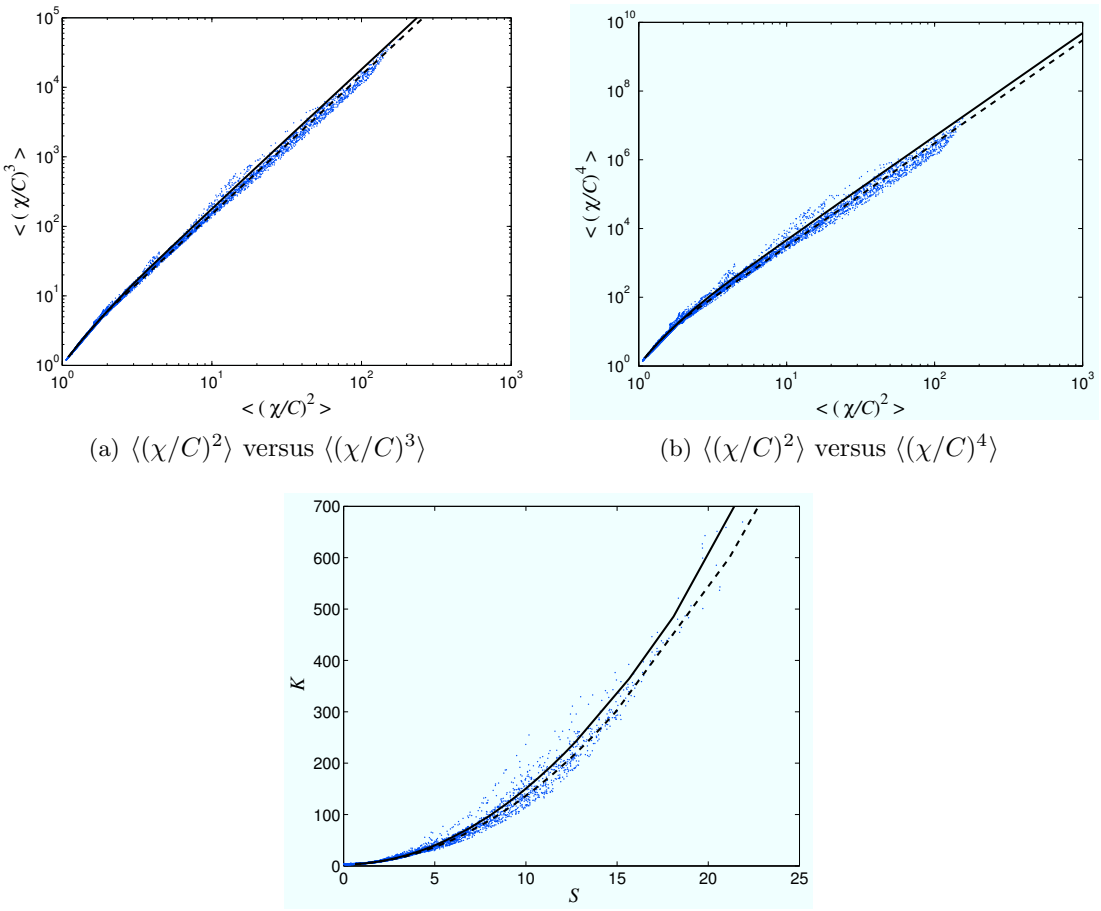

(a) $\langle(\chi/C)^2\rangle$ versus $\langle(\chi/C)^3\rangle$

(b) $\langle(\chi/C)^2\rangle$ versus $\langle(\chi/C)^4\rangle$

(c) S versus K

Figure 10: *Scattergrams of third- and fourth-order normalized concentration moments against the second-order normalized concentration moment and of skewness S against kurtosis K for the URB01 obstacle array with the source located in quadrant C (in a streamwise-oriented street canyon between two columns of obstacles).*

respectively].

For comparative purposes, the theoretical relationships between $\langle(\chi/C)^n\rangle$ $(n = 3, 4)$ and $\langle(\chi/C)^2\rangle$ and between S and K, generated by the clipped-gamma PDF and intermittent exponential PDF, have been superimposed on the scatterplots in Figures 9–18. In all these figures, the solid and dashed curves represent the theoretical curves predicted using the clipped-gamma and intermittent exponential distributions, respectively. It is seen that both the intermittent exponential and clipped-gamma distributions appear to provide rather good fits to the measurements over the full range of conditions covered by the concentration data sets. Even so, it appears that generally the concentration moments are slightly under-predicted by the intermittent exponential distribution (viz., more of the data points in the concentration moment diagrams, and especially in the plots of kurtosis against skewness,

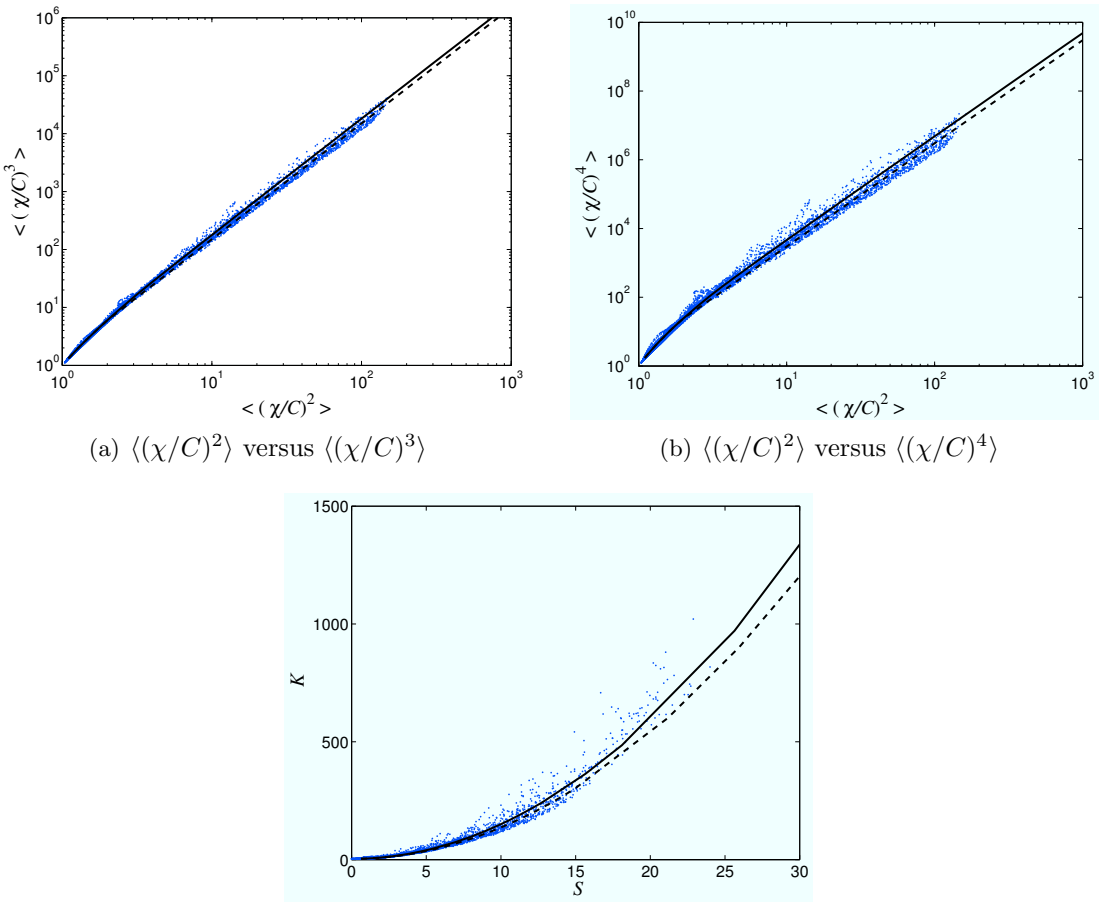

(a) $\langle(\chi/C)^2\rangle$ versus $\langle(\chi/C)^3\rangle$

(b) $\langle(\chi/C)^2\rangle$ versus $\langle(\chi/C)^4\rangle$

(c) S versus K

Figure 11: *Scattergrams of third- and fourth-order normalized concentration moments against the second-order normalized concentration moment and of skewness S against kurtosis K for the URB01 obstacle array with the source located in quadrant D (in a spanwise-oriented street canyon between two rows of obstacles).*

lie slightly above the curve generated by the exponential PDF).

The observed concentration moment relationships for plumes dispersing in various obstacle arrays (summarised in Figures 9–18) are in good agreement with predictions provided by the clipped-gamma PDF. Interestingly, Yee and Chan [14] demonstrated that the clipped-gamma PDF provided predictions of concentration moment relationships that were in very good conformance with the measured concentration moment relationships obtained from the extensive CONFLUX experiments. These experiments provided concentration data for plumes dispersing over level, unobstructed terrain that covered a very wide range in plume positions and atmospheric conditions. Taken together, this implies that the concentration moment relationships for plumes dispersing in the complex urban terrain are identical to those for plumes dispersing in simple (rural) terrain.

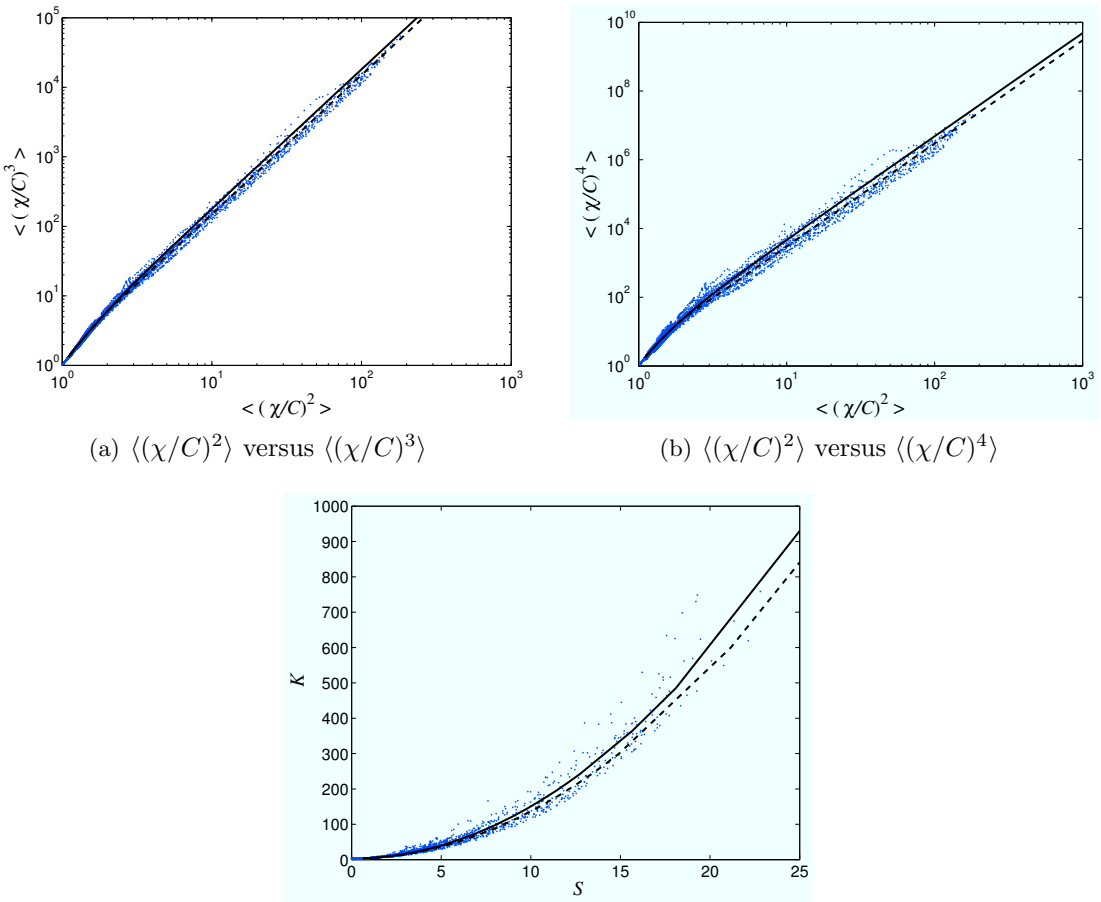

(a) $\langle(\chi/C)^2\rangle$ versus $\langle(\chi/C)^3\rangle$

(b) $\langle(\chi/C)^2\rangle$ versus $\langle(\chi/C)^4\rangle$

(c) S versus K

Figure 12: *Scattergrams of third- and fourth-order normalized concentration moments against the second-order normalized concentration moment and of skewness S against kurtosis K for the URB02 obstacle array with the source located in quadrant C (in a streamwise-oriented street canyon between two columns of obstacles).*

It is known that large groups of obstacles (characteristic of a built-up environment) can have a profound effect on the mean concentration and concentration variance in a dispersing plume in comparison to plume dispersion over open terrain. In an obstacle array, non-Gaussian distributions of mean concentration are possible due to the splitting of plumes into two by the horseshoe vortex that may form around the base of an obstacle. There may be an effective lifting of the mean plume centroid caused by deflection of mean flow streamlines over an array of obstacles. The trajectory of the mean plume centerline in the lateral direction may be offset from the direction of the mean wind aloft due to crosswind channeling of the flow in the array of obstacles. In certain circumstances, channeling of the flow along array passages may inhibit the lateral spread of the mean plume. Alternatively, topological diffusion of the plume due to streamline divergence can lead to an enhanced lateral mean plume spread, whereas rapid vertical mixing in the recirculating wakes behind obstacles

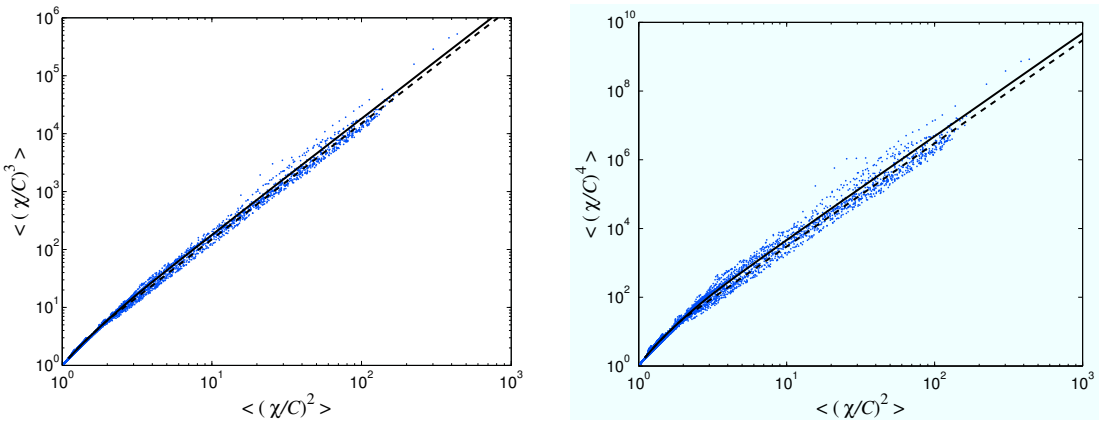

(a) $\langle(\chi/C)^2\rangle$ versus $\langle(\chi/C)^3\rangle$ (b) $\langle(\chi/C)^2\rangle$ versus $\langle(\chi/C)^4\rangle$

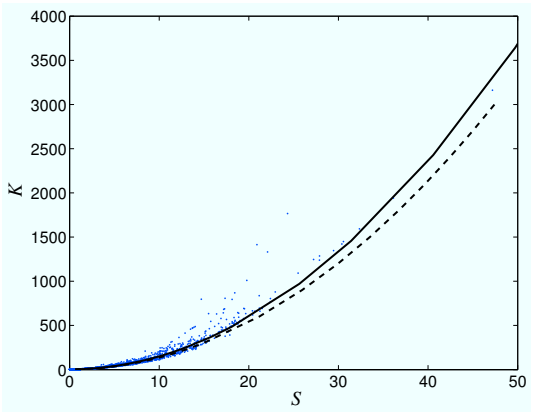

(c) S versus K

Figure 13: *Scattergrams of third- and fourth-order normalized concentration moments against the second-order normalized concentration moment and of skewness S against kurtosis K for the URB02 obstacle array with the source located in quadrant D (in a spanwise-oriented street canyon between two rows of obstacles).*

may lead to an enhanced vertical mean plume spread. These important modifications of the structure of the mean concentration field, in a plume dispersing through an array of obstacles, have been discussed by Davidson et al [23], Macdonald et al [24], and Yee and Biltoft [17].

Yee and Biltoft [17] demonstrated that the second moment of concentration (or, concentration variance) in a plume dispersing through an array of obstacles is reduced, relative to that observed in a comparable plume dispersing over open terrain. This reduction in the concentration variance is the consequence of two physical mechanisms: (1) a significant reduction in the meandering of the instantaneous plume in an obstacle array (relative to an open-terrain plume) due to an observed increase in the lateral spreads of the plume and a reduction in the scale of turbulence between the obstacles in the array, and (2) a significant reduction in concentration variance of the in-plume fluctuations in the array plume

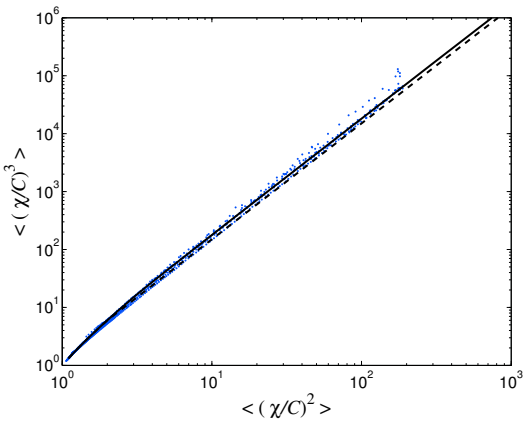

(a) $\langle(\chi/C)^2\rangle$ versus $\langle(\chi/C)^3\rangle$

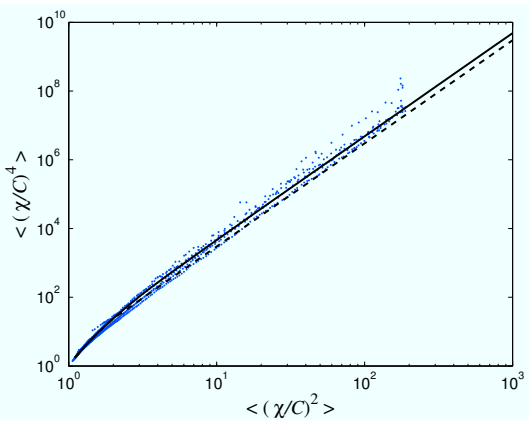

(b) $\langle(\chi/C)^2\rangle$ versus $\langle(\chi/C)^4\rangle$

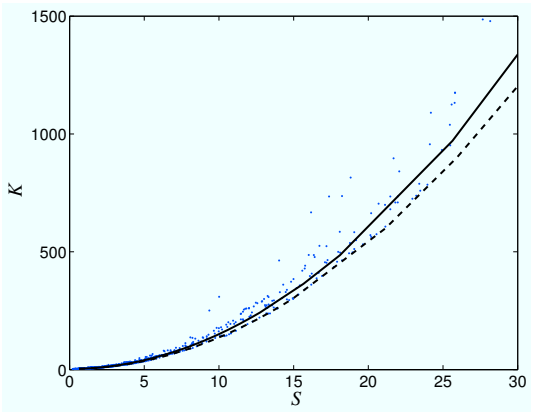

(c) S versus K

Figure 14: *Scattergrams of third- and fourth-order normalized concentration moments against the second-order normalized concentration moment and of skewness S against kurtosis K for the URB03 obstacle array with the source located in quadrant C (in a streamwise-oriented street canyon between two columns of obstacles).*

(in comparison to the open-terrain plume) owing to the enhanced small-scale mixing of the plume material in the high intensity turbulence that is characteristic of the flow within an obstacle array.

In spite of the significant modifications in the structure of a plume dispersing in an obstacle array when compared to an open-terrain plume, the modifications manifest themselves in their effects on the first- and second-order concentration moments (or, equivalently, on the mean concentration and concentration variance). Interestingly, Figures 9–18 seem to suggest that despite the fact that an obstacle array has a significant effect on the first two moments of the concentration, the relationships of the third- and higher-order normalized concentration moments to the second-order normalized concentration moment in an array plume are exactly the same as those observed in an open-terrain plume. This suggests that the plume concentration fluctuation structure in an obstacle array is the same as that which

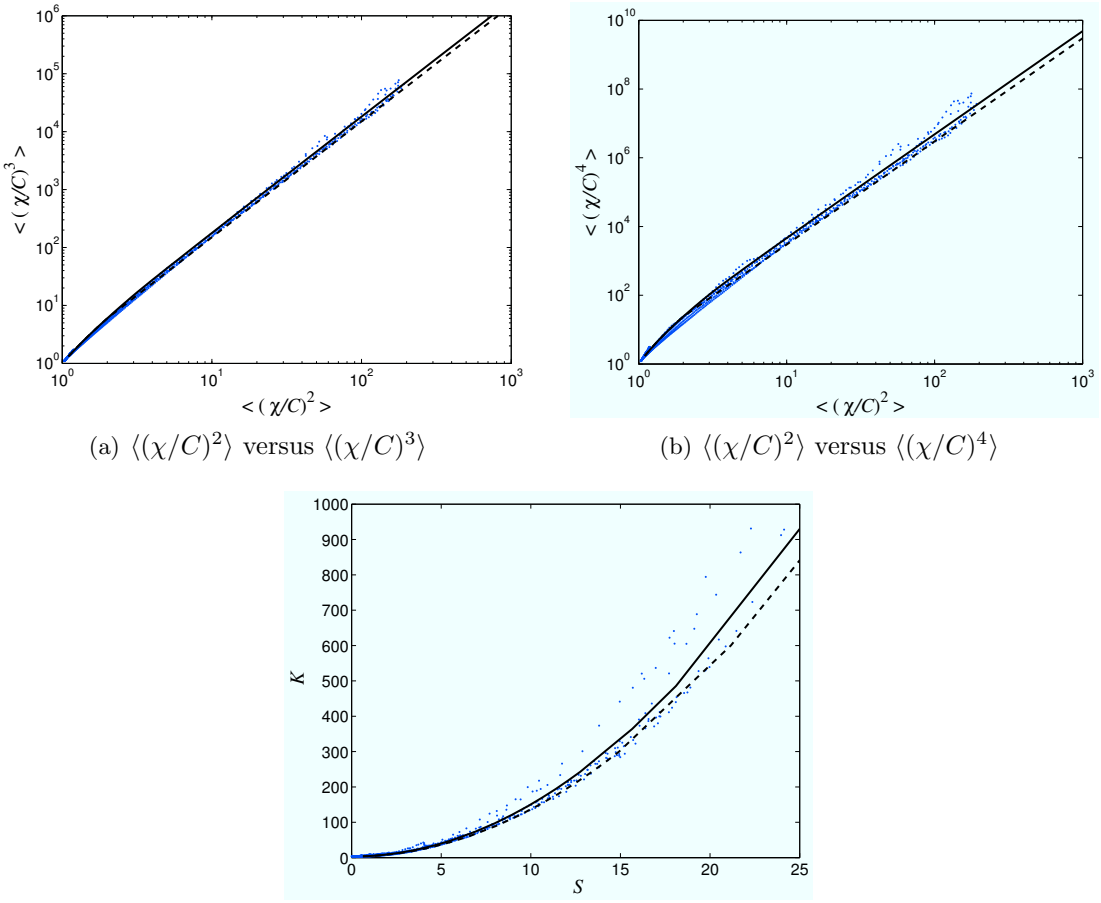

(a) $\langle(\chi/C)^2\rangle$ versus $\langle(\chi/C)^3\rangle$

(b) $\langle(\chi/C)^2\rangle$ versus $\langle(\chi/C)^4\rangle$

(c) S versus K

Figure 15: *Scattergrams of third- and fourth-order normalized concentration moments against the second-order normalized concentration moment and of skewness S against kurtosis K for the URB03 obstacle array with the source located in quadrant D (in a spanwise-oriented street canyon between two rows of obstacles).*

would be observed in an open-terrain plume at a much greater distance downwind when the instantaneous plume has grown to fill the mean-plume width (hence, dramatically reducing the contribution of large-scale meander to the concentration fluctuations) and when the continuous molecular mixing has had a chance to smooth out the in-plume fluctuations. The latter effect on the structure of an open-terrain plume is identical to the effect of the more rapid, homogeneous mixing in an array plume due to the small-scale, high-intensity turbulence that is characteristic of the flow within an obstacle array. This explains why the concentration moment relationships observed in an array plume are identical (approximately or better) to those observed in an open-terrain plume.

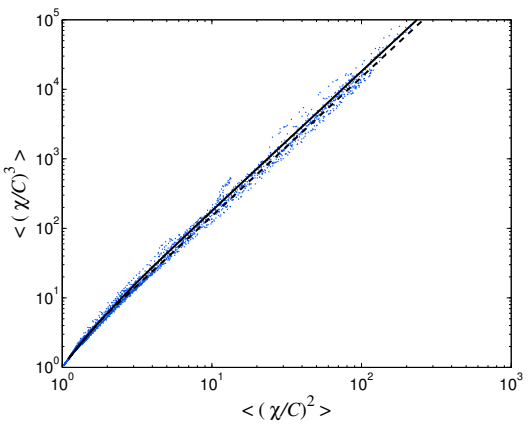

(a) $\langle(\chi/C)^2\rangle$ versus $\langle(\chi/C)^3\rangle$

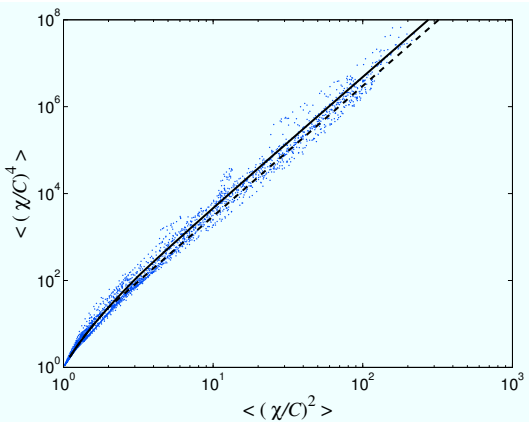

(b) $\langle(\chi/C)^2\rangle$ versus $\langle(\chi/C)^4\rangle$

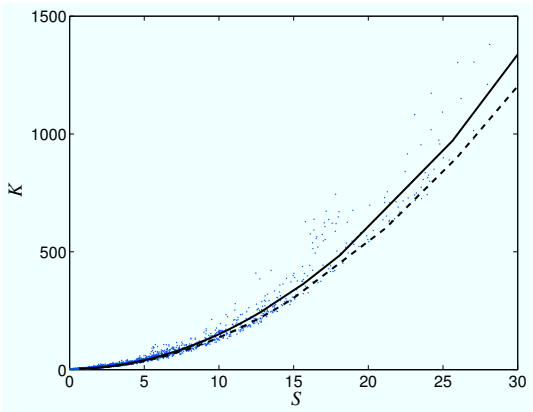

(c) S versus K

Figure 16: *Scattergrams of third- and fourth-order normalized concentration moments against the second-order normalized concentration moment and of skewness S against kurtosis K for the URB04 obstacle array with the source located in quadrant D (in a spanwise-oriented street canyon between two rows of obstacles).*

5 Concentration PDF

In this section, we compare the shape of the model probability distributions to the observed concentration data at a number of plume locations for two of the obstacle arrays. The concentration probability distribution embodies the information required to predict the probability of exposure to high concentrations and, as such, contains the information on all the moments of the fluctuating plume concentration. This information can be used to derive all one-point statistics of the concentration field.

To this end, we extract the cumulative and exceedance probability distributions from the array plume concentration data and compare these measured distributions to two model cumulative and exceedance probability distributions; namely, to the clipped-gamma and

intermittent exponential distributions. In view of Eqs. (2) and (15), the cumulative distribution function for the concentration at a fixed receptor point can be written as

$$F(c;\mathbf{x},t) = \gamma F^{+}(c;\mathbf{x},t) + (1-\gamma)H(c;\mathbf{x},t), \tag{22}$$

where $F^{+}(c;\mathbf{x},t)$ is the probability distribution for the in-plume concentration fluctuations and $H(c;\mathbf{x},t)$ is a unit step function with a step at $c = 0$ of magnitude $(1-\gamma)$, which expresses the probability of observing zero concentration at receptor location $\mathbf{x}$ at time t. For the clipped-gamma distribution [cf. Eq. (2)],

$$\begin{aligned} F(c;\mathbf{x},t) &\equiv \int_{0^-}^{c} f(c';\mathbf{x},t)\,dc' \\ &= 1 - \frac{\Gamma(k;(c+\lambda)/s)}{\Gamma(k)}. \end{aligned} \tag{23}$$

Similarly, for the intermittent exponential distribution,

$$\begin{aligned} F(c;\mathbf{x},t) &\equiv \int_{0^-}^{c} f(c';\mathbf{x},t)\,dc' \\ &= 1 - \gamma \exp\left(-\frac{\gamma c}{C}\right), \end{aligned} \tag{24}$$

where γ is determined by Eq. (19). Observe from Eqs. (23) and (24) that

$$F(0^{-};\mathbf{x},t) = 1-\gamma, \tag{25}$$

is the probability of observing zero concentration at receptor location $\mathbf{x}$ and time t.

Figure 19 presents measured cumulative distribution functions (CDFs) of the normalized concentration c/C obtained at five different downstream locations along the mean plume centerline at half canopy height for dispersion in the MUST obstacle array. The clipped-gamma (solid line) and intermittent exponential (dashed line) distributions, with the same normalized mean-squared concentration $\langle(\chi/C)^2\rangle$ as the measured result, are also exhibited in Figure 19 for comparison. The clipped-gamma distribution is seen to be to in excellent conformance with the measured concentration CDFs at the various downstream locations. However, the intermittent exponential distribution provides a very poor fit to the measured concentration CDFs. More specifically, the lower tail of the intermittent exponential distribution is much heavier than that for the observed concentration CDF (viz., the intermittent exponential distribution predicts a larger probability for non-exceedances of small concentration levels with $c/C < 1$ than that given by the observed values).

Generally, for a number of practical applications, it is the largest peak concentrations that are of greatest interest. Because it is the prediction of the likelihood of extreme events that is important in the hazard assessment of toxic gas releases, it is important to examine the upper tail of the concentration distributions. To that purpose, we display in Figure 20 the exceedance probability distributions, $1-F(c/C)$, for the same plume locations shown in Figure 19 for dispersion in the MUST obstacle array. The exceedance probability distributions have been plotted on a logarithmic scale in order to emphasize the upper tails.

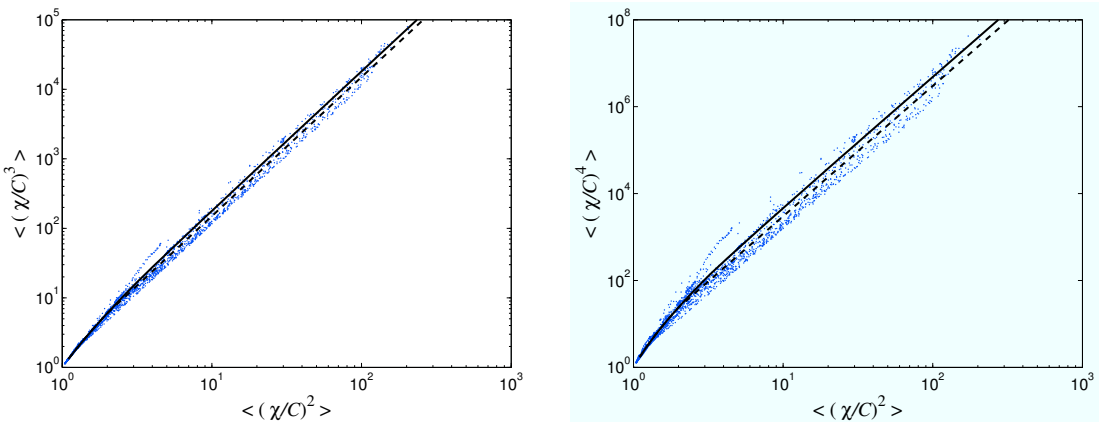

(a) $\langle(\chi/C)^2\rangle$ versus $\langle(\chi/C)^3\rangle$

(b) $\langle(\chi/C)^2\rangle$ versus $\langle(\chi/C)^4\rangle$

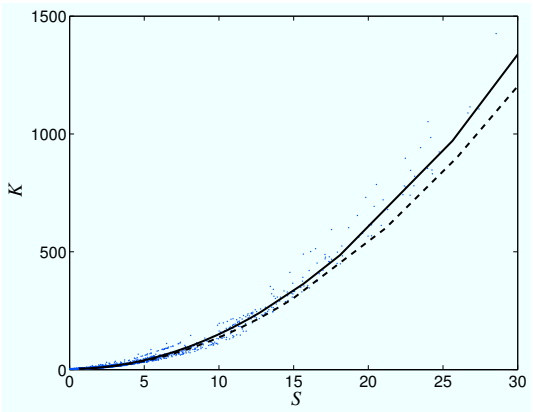

(c) S versus K

Figure 17: *Scattergrams of third- and fourth-order normalized concentration moments against the second-order normalized concentration moment and of skewness S against kurtosis K for the URB10 obstacle array with the source located in quadrant C (in a streamwise-oriented street canyon between two columns of obstacles).*

Figure 20 indicates that the clipped-gamma distribution predicts the upper tail extremely well. In contrast, the intermittent exponential distribution exhibits considerably longer upper tails than the observed concentration probability distribution. This implies that the intermittent exponential distribution tends to overpredict (significantly) the probability of occurrence of large concentrations ($c/C > 1$).

As another example, Figures 21 and 22 exhibit the measured CDFs and EDFs, respectively, of the normalized concentration c/C obtained at six different downstream locations at half canopy height ($z/H = 0.5$) along the mean centerline for the plume dispersing in the URB01 obstacle array with the source located in quadrant D. Additionally, these figures show the curves provided by the clipped-gamma (solid line) and intermittent exponential (dashed lines) distributions, which were generated using the measured mean-square concentration $\langle(\chi/C)^2\rangle$ obtained at each of these plume locations. Again, it can be seen that the

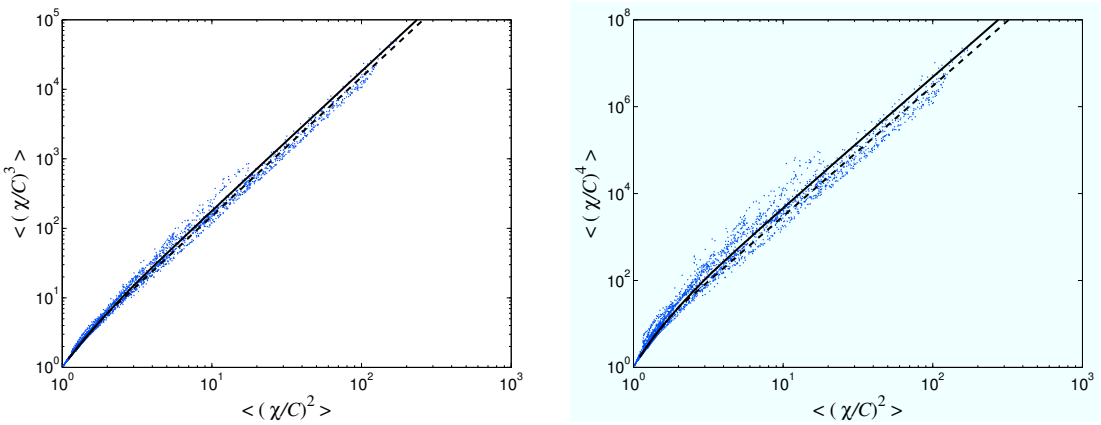

(a) $\langle(\chi/C)^2\rangle$ versus $\langle(\chi/C)^3\rangle$

(b) $\langle(\chi/C)^2\rangle$ versus $\langle(\chi/C)^4\rangle$

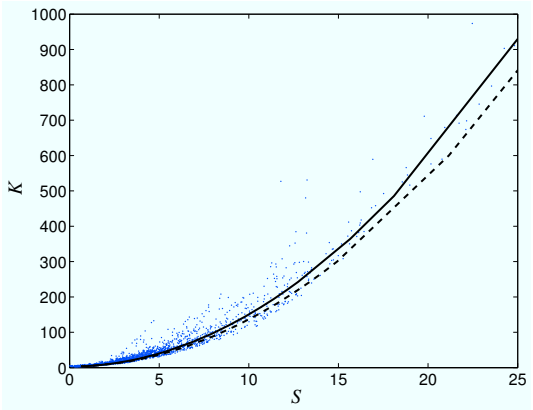

(c) S versus K

Figure 18: *Scattergrams of third- and fourth-order normalized concentration moments against the second-order normalized concentration moment and of skewness S against kurtosis K for the URB10 obstacle array with the source located in quadrant D (in a spanwise-oriented street canyon between two rows of obstacles).*

clipped-gamma distribution provides very good predictions for the shape of the measured concentration probability distributions. More importantly, the extent of the upper tails of the concentration probability distributions are predicted very well using the clipped-gamma distribution. In contrast, the intermittent exponential distribution is seen to provide rather poor predictions for the measured concentration probability distribution. This model distribution tends to overpredict the probability of non-exceedances of small concentration levels ($c/C < 1$) and exceedances of large concentration levels ($c/C > 1$).

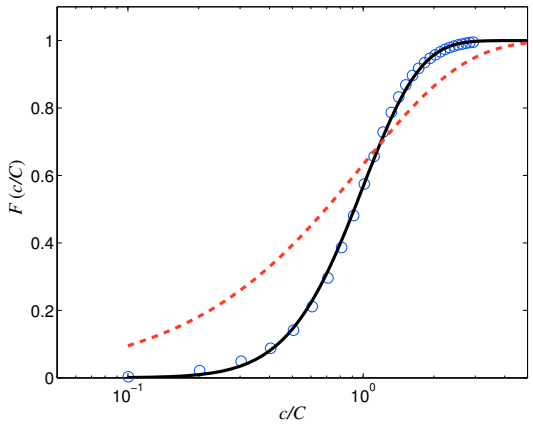

(a) Plume centerline at row 2.5

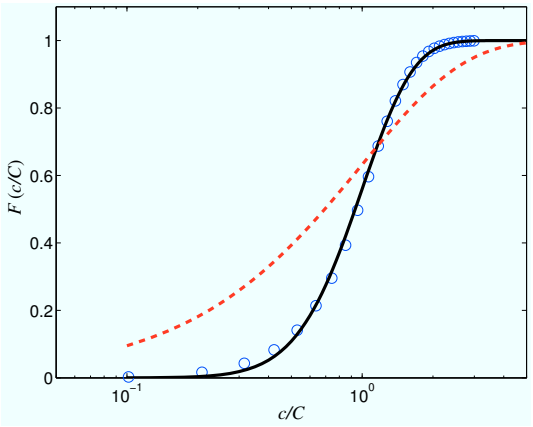

(b) Plume centerline at row 3.5

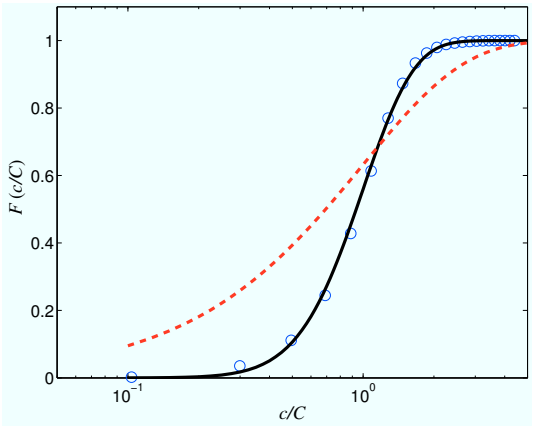

(c) Plume centerline at row 4.5

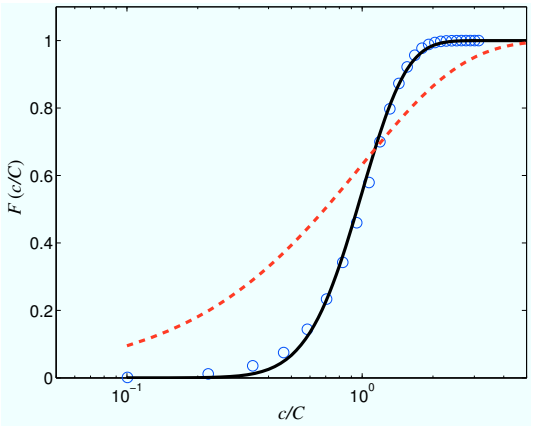

(d) Plume centerline at row 6.5

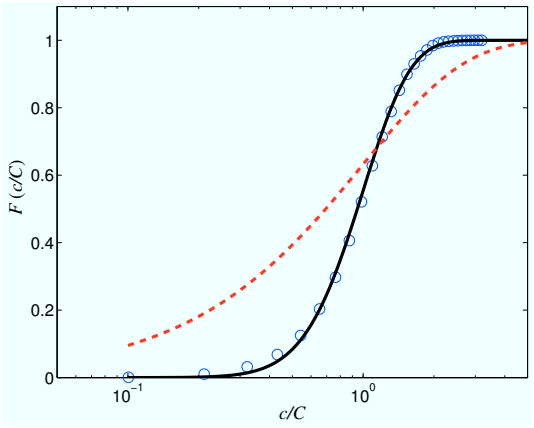

(e) Plume centerline at row 9.5

Figure 19: *Cumulative distribution function (CDF), $F(c/C)$, of the normalized concentration measured at various receptor positions at half canopy height along the mean centerline of a plume dispersing in the MUST obstacle array.*

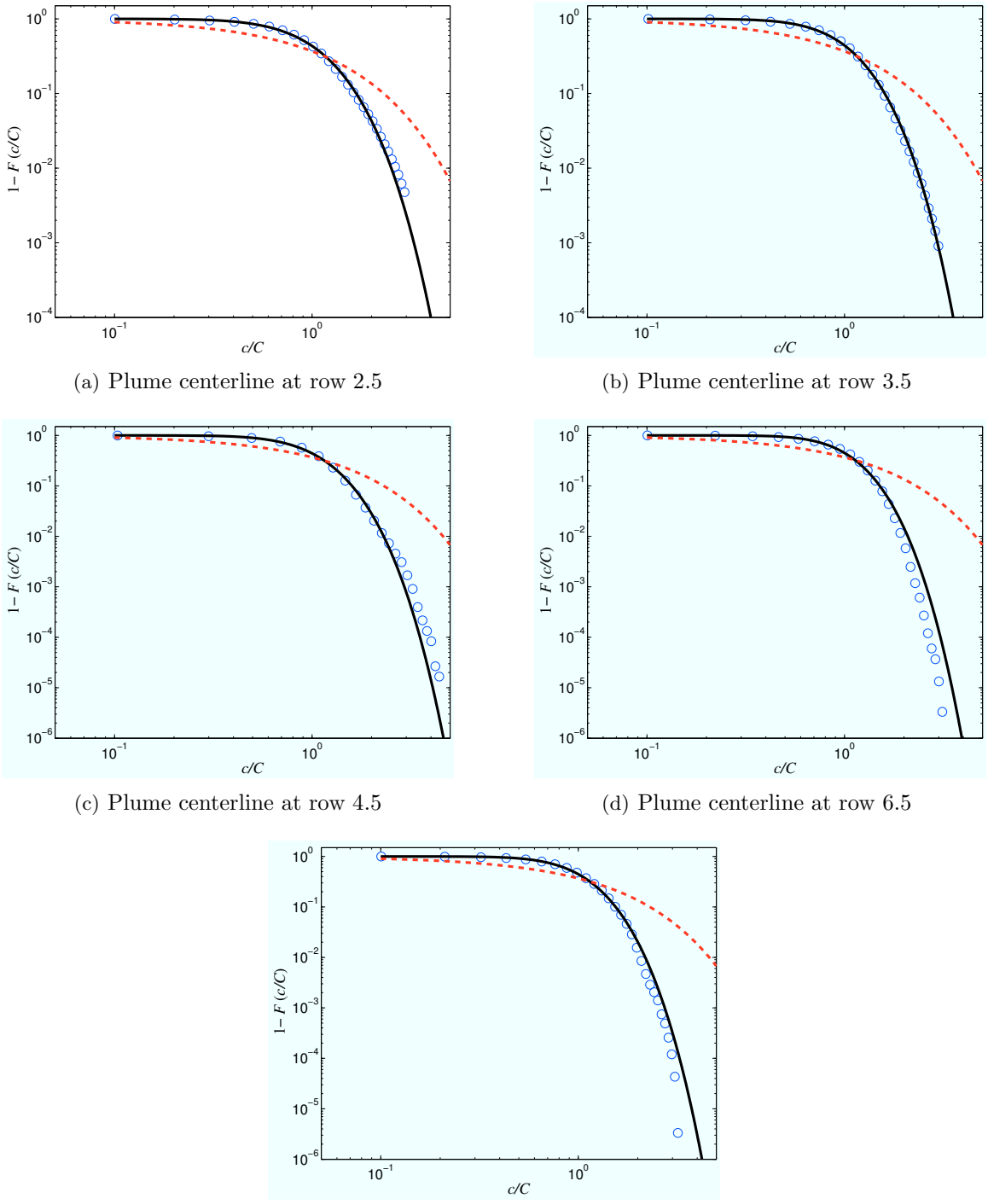

(a) Plume centerline at row 2.5

(b) Plume centerline at row 3.5

(c) Plume centerline at row 4.5

(d) Plume centerline at row 6.5

(e) Plume centerline at row 9.5

Figure 20: *Exceedance distribution function (EDF),* $1 - F(c/C)$*, of the normalized concentration measured at various receptor positions at half canopy height along the mean centerline of a plume dispersing in the MUST obstacle array.*

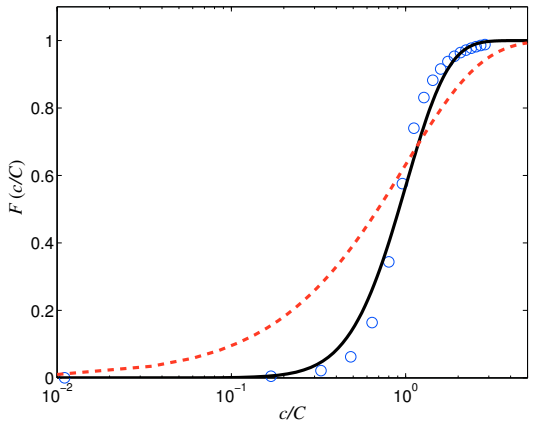

(a) Plume centerline at row 2.5

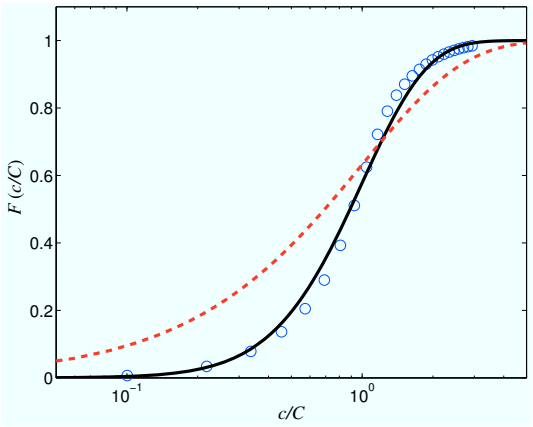

(b) Plume centerline at row 3.5

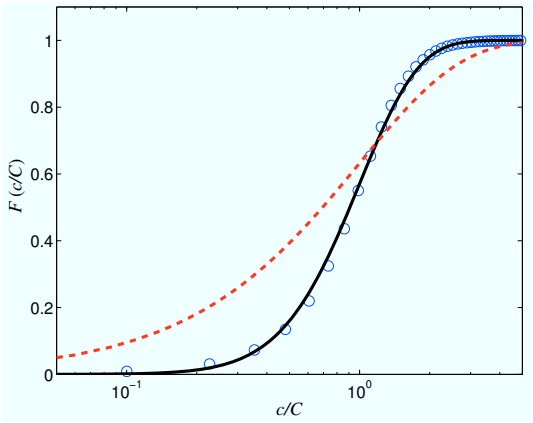

(c) Plume centerline at row 4.5

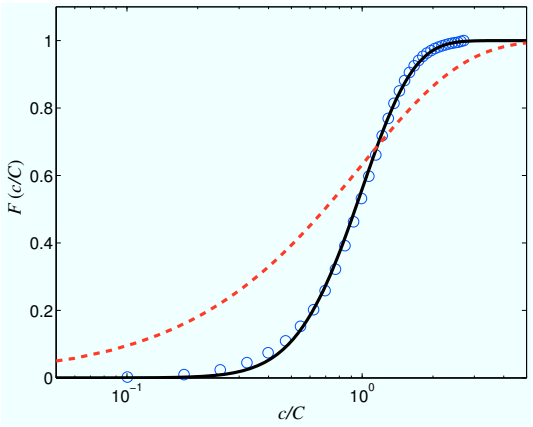

(d) Plume centerline at row 6.5

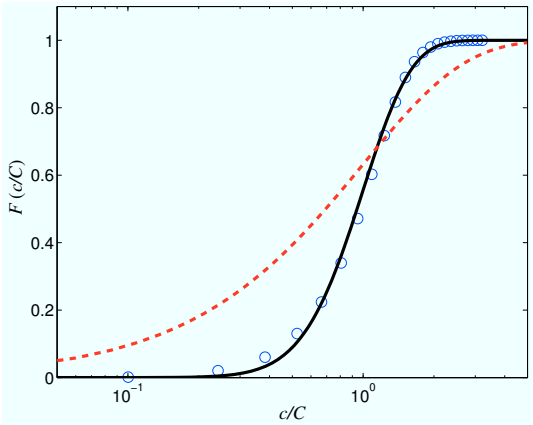

(e) Plume centerline at row 9.5

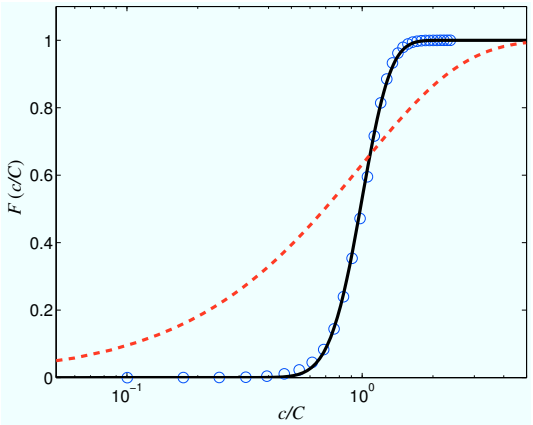

(f) Plume centerline at row 14.5

Figure 21: *Cumulative distribution function (CDF), $F(c/C)$, of the normalized concentration measured at various receptor positions at half canopy height along the mean centerline of a plume dispersing in the URB01 obstacle array with the source in quadrant D.*

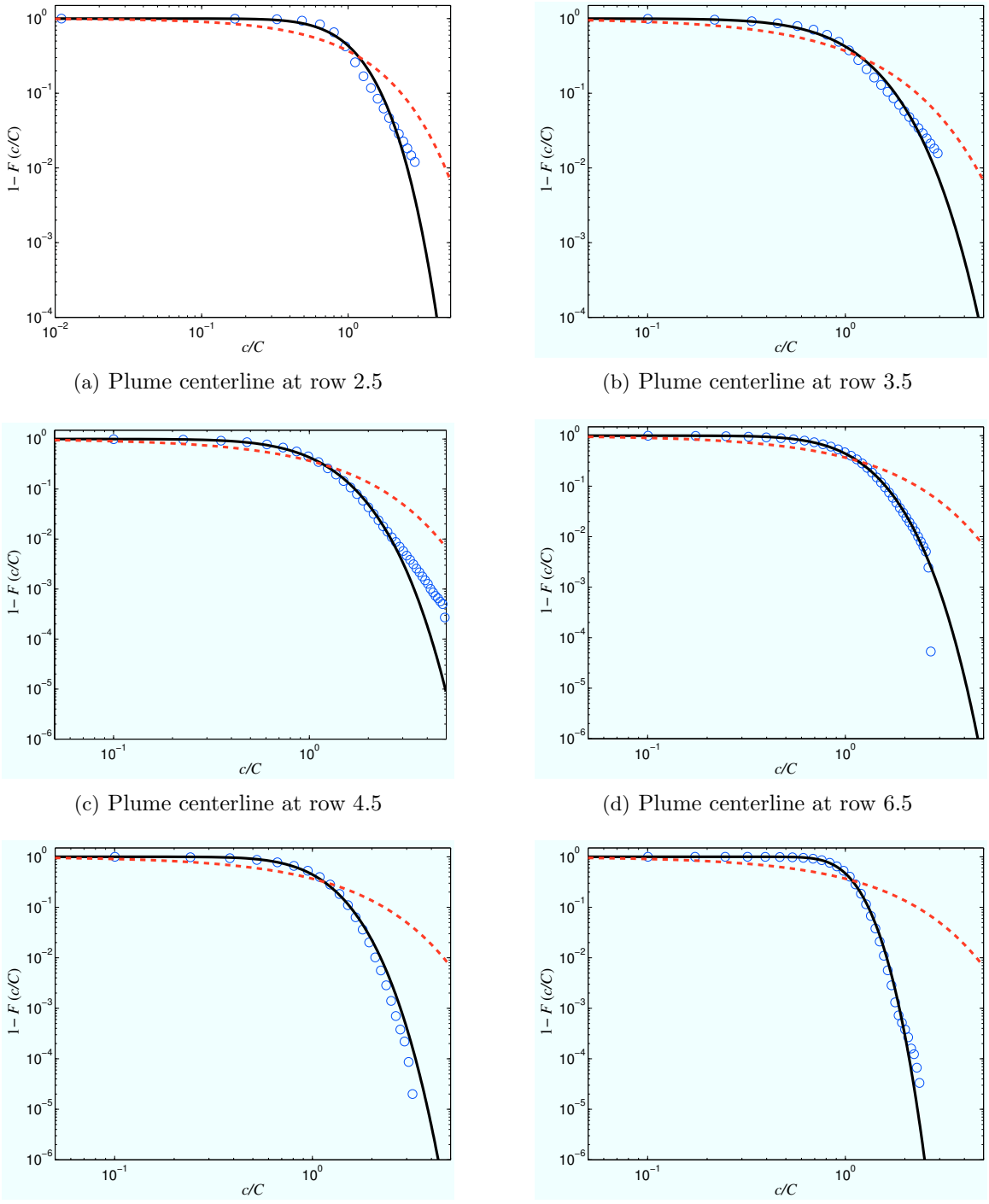

(a) Plume centerline at row 2.5

(b) Plume centerline at row 3.5

(c) Plume centerline at row 4.5

(d) Plume centerline at row 6.5

(e) Plume centerline at row 9.5

(f) Plume centerline at row 14.5

Figure 22: *Exceedance distribution function (EDF),* $1 - F(c/C)$*, of the normalized concentration measured at various receptor positions at half canopy height along the mean centerline of a plume dispersing in the URB01 obstacle array with the source in quadrant* D*.*

6 Implications for sensor modeling

A critical capability gap in current emergency and retrospective management efforts, directed at terrorist incidents involving the covert release of a chemical, biological and radiological (CBR) agent in a densely populated urban center, is the localization of the unknown source(s) following event detection by an array of independent CBR sensors. A considerable research effort has been undertaken in the past two years to develop a methodology to address the inverse prediction of agent source location and strength using a finite number of noisy concentration measurements obtained from an array of CBR detectors. To this purpose, Bayesian probabilistic inference has been applied successfully to the problem of source resconstruction in complex environmental conditions (e.g., complex and/or urban terrain involving highly disturbed wind fields exhibiting a significant degree of spatial inhomogeneity and/or temporal non-stationarity) [25], [26], [27].

In the studies of source reconstruction cited here, the time-averaged (or, ensemble) mean concentration measured at the sensor location was used for the source reconstruction, representing the mean of either a number of realizations of concentration or concentrations averaged over periods of time of several minutes or hours. However, many detectors provide measurements of concentration occurring on time scales of a few seconds or less, not the average over minutes or hours. Moreover, many of these detectors only provide short time-averaged concentrations that have been discretized into a small number of amplitude levels (or, bars). For example, the Chemical Agent Monitor (CAM) which uses ion mobility spectrometry (Smiths Detection) and the AP4C chemical detector which uses flame spectrophotometry (Proengin Inc.) are hand-held chemical warfare agent field detectors that report short time-averaged concentration levels discretized on an eight- and five-bar scale, respectively.

In order to use this type of concentration information for source reconstruction, we need a description of the concentration fluctuations, as well as the ensemble mean concentration in the formulation of the problem. Indeed, a chemical agent detector with a short averaging time (less than tens of seconds) placed at a fixed position downwind of a release of a contaminant will experience concentration fluctuations because of plume sweeping and small-scale turbulent mixing. These fluctuations can deviate significantly from the mean concentration value, and models for the response of these sensors must account properly for the effects of random concentration fluctuations in hazardous gas releases. The purpose of this section is to show how this can be accomplished.

A key quantity required for Bayesian source inversion is the likelihood function which encodes all the information provided by the concentration data about the unknown contaminant source. The likelihood function provides a measure of how likely the concentration measurements made by a detector (e.g., CAM, AP4C) would be for a given source distribution. We will now show how to formulate a likelihood function for a chemical agent detector, such as the CAM or AP4C, in terms of the concentration PDF which provides the one-point statistical information about the instantaneous plume or cloud concentration.

A chemical agent bar sensor will exhibit a bar level b_i ($i = 1, 2, \ldots, N_b$ where N_b is the

maximum number of bar levels), if the measured concentration at the receptor location $\mathbf{x}$ averaged over a short time window (typically between about 5–10 s) centered at time t, lies in the concentration semi-open interval $(c_i^<, c_i^>]$. Here, $c_i^<$ and $c_i^>$ are the lower and upper bounds, respectively, of the concentration that defines the i-th bar level for a chemical agent detector. In other words, the chemical agent detector will issue a "reading" for the i-th bar level b_i if the measured concentration $c_m \in (c_i^<, c_i^>]$. Now, we can apply the product rule of probability calculus to obtain the following expression for the probability that a bar level b_i is observed by a chemical agent detector, conditioned on a release from a given source distribution S:[6]

$$p(b_i) = \int_{c_i^<}^{c_i^>} \int_0^\infty \int_0^\infty \int_0^\infty f(c_m|c) f(c|C, \overline{c^2}) f(C|S) f(\overline{c^2}|S)\, d\overline{c^2}\, dC\, dc\, dc_m, \tag{26}$$

for $i = 1, 2, \ldots, N_b$. In Eq. (26), $f(c_m|c)$ is the probability density function of the measured concentration c_m conditioned on the true (unknown) concentration c; $f(c|C, \overline{c^2})$ is the concentration PDF, which is implicitly assumed to depend on two parameters (namely, the mean concentration C and the mean-square concentration $\overline{c^2}$)[7]; $f(C|S)$ is the PDF for C given the source distribution S; and, $f(\overline{c^2}|S)$ is the PDF for $\overline{c^2}$ given the source distribution S. Next, we consider the specification or assignment of each of these component PDFs.

First, let us consider the assignment of $f(c_m|c)$. If the true (unknown) concentration is c, then the measured concentration datum c_m is given by

$$c_m = c + \epsilon_1, \tag{27}$$

where ϵ_1 represents the measurement (detector) noise, which includes the effects of digitization errors, calibration errors, and shot noise. It is assumed that the measurement error ϵ_1 is known to have zero mean and variance σ_1^2. The principle of maximum entropy provides a powerful criterion for formulation of a prior noise probability density function that encodes our state of knowledge about the measurement noise ϵ_1 (see Jaynes [28] for an insightful discussion of the maximum entropy principle). Application of the principle of maximum entropy informs us that a Gaussian distribution is the most conservative choice for the PDF of ϵ_1, or equivalently, for $f(c_m|c)$:

$$f(c_m|c) \equiv f(c_m|c, \sigma_1^2) = \frac{1}{\sqrt{2\pi\sigma_1^2}} \exp\left(-\frac{(c_m - c)^2}{2\sigma_1^2}\right), \tag{28}$$

where the explicit dependence of $f(c_m|c)$ on σ_1^2 has been indicated. It should be noted that any other noise PDF will have more compact support (lower entropy) than the Gaussian given the finite noise power σ_1^2; thus, the assignment of the Gaussian form for the noise PDF will give the most conservative representation for the structure of the measurement noise.

[6] The dependence of various quantities on $\mathbf{x}$ and t has been suppressed to simplify the notation. Furthermore, the conditioning of the probability $p(b_i)$ on the source distribution S has been suppressed in the notation.

[7] This corresponds to a slight abuse of the notation used earlier, in which the mean-square concentration was denoted as $\langle \chi^2 \rangle$ [cf. Eq. (7)]. Hence, in this section, the identification $\overline{c^2} \equiv \langle \chi^2 \rangle$ should be made.

Next, let us focus on specification of the concentration PDF $f(c|C,\overline{c^2})$. In a previous section, it was shown that the form of the concentration PDF can be specified using only two parameters, and that the clipped-gamma distribution fits the concentration observations very well. In consequence, we can assign a clipped-gamma distribution for $f(c|C,\overline{c^2})$. By virtue of Eqs. (2), (3) and (10), the concentration PDF $f(c|C,\overline{c^2})$ can be explicitly expressed as follows:[8]

$$f(c|C,\overline{c^2}) = \left(\frac{c+\lambda}{s}\right)^{k-1} \frac{\exp\big(-(c+\lambda)/s\big)}{s\Gamma(k)} + (1-\gamma)\delta(c), \tag{29}$$

where

$$\gamma \equiv \min\left(1, \frac{3C^2}{\overline{c^2}}\right) = \frac{\Gamma(k;\lambda/s)}{\Gamma(k)}. \tag{30}$$

It should be stressed that k, s, λ is uniquely determined from a knowledge of C and $\overline{c^2}$. More specifically, the latter quantities determine the normalized mean-square concentration $\overline{c^2}/C^2 \equiv \langle(\chi/C)^2\rangle$, and as exhibited in Figure 1, the parameters k, s, and λ of the clipped-gamma distribution are uniquely specified given the value of $\overline{c^2}/C^2$.

Next, let us consider $f(C|S)$. The true mean concentration C, at the location of the chemical agent detector, resulting from the release of a contaminant from a given source distribution S is not known. This quantity needs to be estimated using an atmospheric dispersion model (e.g., C can be estimated using either a Gaussian puff or a one-particle Lagrangian stochastic trajectory simulation model). Hence, $f(C|S)$ specifies the uncertainty in the estimation of C using a dispersion model for a hazardous gas release from a given source distribution S. To this purpose, we first assume that the predicted (or, model) mean concentration C_p, obtained from an atmospheric dispersion model, provides an unbiased estimate for the true (unknown) mean concentration C. The one standard deviation uncertainty in the estimate C_p for C is σ_2, the latter of which is assumed to be known.[9] This uncertainty arises from model errors in the representation of various physical processes in the dispersion model used to predict the mean concentration and input errors in the values of empirical parameters and/or specification of the input meteorology (initial and boundary conditions) used by the dispersion model. Next, we assume that $f(C|S)$ can be specified by a gamma distribution with mean C_p and standard deviation σ_2, so

$$f(C|S) \equiv f(C|S,C_p,\sigma_2) = \frac{C^{C_p^2/\sigma_2^2-1}\exp\big(-CC_p/\sigma_2^2\big)}{\big(\sigma_2^2/C_p\big)^{C_p^2/\sigma_2^2}\Gamma(C_p^2/\sigma_2^2)}, \tag{31}$$

where the explicit dependence of $f(C|S)$ on C_p and σ_2 has been indicated.

Finally, we consider the assignment of $f(\overline{c^2}|S)$ which encodes the uncertainty in our prediction of the mean-square concentration $\overline{c^2}_p$ for a hazardous gas release from a given source distribution S, the true value of the mean-square concentration $\overline{c^2}$ being unknown. The mean-square concentration can be modeled using a fluctuating plume model [29], [30] or

[8] Recall that for the clipped-gamma distribution, when $\overline{c^2}/C^2 \leq 3$ the intermittency factor is set equal to unity identically and this distribution reduces to the usual gamma distribution under these circumstances.

[9] Normally, the expected uncertainty in the prediction of the mean concentration using a dispersion model is available from model validation (evaluation) exercises conducted with benchmark dispersion data sets.

a second-order closure model [31], [21]. The predicted (model) mean-square concentration $\overline{c^2}_p$ is assumed to be an unbiased estimate for the true (unknown) mean-square concentration $\overline{c^2}$. The one standard deviation uncertainty in the estimate $\overline{c^2}_p$ for $\overline{c^2}$ is σ_3, the latter providing the scale of the uncertainty in the determination of the true mean-square concentration arising from model and input errors. Furthermore, it is assumed that $f(\overline{c^2}|S)$ can be specified by gamma distribution with mean $\overline{c^2}_p$ and standard deviation σ_3, so

$$f(\overline{c^2}|S) \equiv f(\overline{c^2}|S, \overline{c^2}_p, \sigma_3) = \frac{\overline{c^2}^{(\overline{c^2}_p)^2/\sigma_3^2 - 1} \exp\left(-\overline{c^2}\,\overline{c^2}_p/\sigma_3^2\right)}{\left(\sigma_3^2/\overline{c^2}_p\right)^{(\overline{c^2}_p)^2/\sigma_3^2} \Gamma((\overline{c^2}_p)^2/\sigma_3^2)}, \tag{32}$$

where the explicit dependence of $f(\overline{c^2}|S)$ on $\overline{c^2}_p$ and σ_3 has been indicated.

Now, we can insert Eq. (28) into Eq. (26) and integrate with respect to c_m to simplify the form for $p(b_i)$. This gives

$$\begin{aligned} p(b_i) \;=\; & \int_0^\infty \int_0^\infty \int_0^\infty \frac{1}{2}\left[\operatorname{erf}\left(\frac{c_i^> - c}{\sqrt{2}\sigma_1}\right) - \operatorname{erf}\left(\frac{c_i^< - c}{\sqrt{2}\sigma_1}\right)\right] \times \\ & f(c|C, \overline{c^2}) f(C|S) f(\overline{c^2}|S)\, d\overline{c^2}\, dC\, dc, \end{aligned} \tag{33}$$

where $\operatorname{erf}(x)$ denotes the error function. Usually, the model and input errors in the prediction of C and $\overline{c^2}$ are much larger than the errors in the measurement of c. In this case, $\sigma_1 \ll \sigma_2,\ \sigma_3$, so that $f(c_m|c)$ in Eq. (28) can be considered to be so sharply peaked about the true concentration c that the function can be reasonably approximated as a delta function:

$$f(c_m|c) = \lim_{\sigma_1 \to 0^+} \frac{1}{\sqrt{2\pi\sigma_1^2}} \exp\left(-\frac{(c_m - c)^2}{2\sigma_1^2}\right) = \delta(c_m - c), \tag{34}$$

so that as $\sigma_1 \to 0^+$ in Eq. (28), the approximation of $f(c_m|c)$ using a delta function becomes exact. With the approximation for $f(c_m|c)$ given by Eq. (34), the form for $p(b_i)$ given by Eq. (26) simplifies to (on noting that $c_m \equiv c$ for this case)

$$p(b_i) = \int_{c_i^<}^{c_i^>} \int_0^\infty \int_0^\infty f(c|C, \overline{c^2}) f(C|S) f(\overline{c^2}|S)\, d\overline{c^2}\, dC\, dc. \tag{35}$$

For the case where the measurement error is assumed to be neglible with respect to the model and input errors, insertion of the functional form for the concentration PDF given by Eq. (29) into Eq. (35) and performing the integration with respect to c yields

$$p(b_i) = \int_0^\infty \int_0^\infty \left[\frac{\Gamma\big(k; (c_i^< + \lambda)/s\big) - \Gamma\big(k; (c_i^> + \lambda)/s\big)}{\Gamma(k)}\right] f(C|S) f(\overline{c^2}|S)\, d\overline{c^2}\, dC, \tag{36}$$

for $i = 1, 2, \ldots, N_b$. The remaining integrations with respect to C and $\overline{c^2}$ in Eq. (36) cannot be evaluated analytically and will need to be evaluated numerically. Note in Eq. (36) that k, s, and λ are implicit functions of C and $\overline{c^2}$ (more specifically, of $\langle(\chi/C)^2\rangle \equiv \overline{c^2}/C^2$) as shown in Figure 1.

The bar levels b_i ($i = 1, 2, \ldots, N_b$) correspond to non-zero bar "readings". A zero bar reading, which we designate using b_0, corresponds to the case when the concentration level is less than $c_1^<$ (lower bound defining the first bar level). For consistency with our previous notation for non-zero bar levels, the zero bar "reading" would be associated with the probability that the concentration c lies in the interval $c_0^< \to 0^-$ and $c_0^> \to c_1^<$. For this special case, the Dirac delta function term in Eq. (29) would contribute to the integral over c in Eq. (35). Consequently, for this case, the probability that the detector would report a zero bar reading (corresponding to a "nominal" zero concentration) is given by

$$p(b_0) = \int_0^\infty \int_0^\infty \left[\frac{\Gamma\big(k; \lambda/s\big) - \Gamma\big(k; (c_1^< + \lambda)/s\big)}{\Gamma(k)} \right] f(C|S) f(\overline{c^2}|S)\, d\overline{c^2}\, dC + \int_0^\infty \int_0^\infty (1-\gamma)\, f(C|S) f(\overline{c^2}|S)\, d\overline{c^2}\, dC, \tag{37}$$

where γ is defined by Eq. (30). The double integrations in Eq. (37) will need to be evaluated numerically.

It should be noted that $p(b_i)$ ($i = 0, 1, 2, \ldots, N_d$) given by Eqs. (36) and (37) should be identified with the likelihood $\mathcal{L}(b_i|S)$ that a detector reports the bar level b_i for a hazardous gas release associated with a given source distribution S. This likelihood function accounts fully for uncertainties in model predictions for C and $\overline{c^2}$, required in the specification of the concentration PDF. More specifically and succinctly, $\mathcal{L}(b_i|S) \equiv p(b_i)$ ($i = 0, 1, 2, \ldots, N_b$). This quantity can be used for the likelihood function in a Bayesian source inversion scheme involving concentration measurements made by a chemical agent detector that outputs only a discrete level bar reading (rather than a continuous level concentration reading).

It was not mentioned previously, but the determination of $p(b_i)$ given by Eq. (26) requires information on the concentration moments C and $\overline{c^2}$ as perceived by the detector (viz., the concentration moments as measured by a detector with the averaging time τ_a). Time-averaging, such as that imposed by a slower response detector, does not affect the mean concentration C (viz., C is invariant to a time-averaging operation). However, the time-averaging inherent in the detector response will affect the mean-square concentration $\overline{c^2}$, owing to the fact that time-averaging will smooth out the fine structure of rapid fluctuations in the concentration time series measured by the detector.

The effects of averaging time on the expected reduction in the concentration variance $\overline{c'^2} \equiv \overline{c^2} - C^2$ has been discussed in Hanna [32] — namely, the variance of concentration fluctuations at a receptor point, averaged over time τ_a, is related to the concentration variance with no time averaging (viz., zero averaging time) as follows:

$$\frac{\overline{c'^2}|_{\tau_a}}{\overline{c'^2}} = 2\frac{T_c}{\tau_a}\left[1 - \frac{T_c}{\tau_a}\big(1 - \exp(-\tau_a/T_c)\big)\right], \tag{38}$$

where $\overline{c'^2}|_{\tau_a}$ is the concentration variance perceived by a detector with an intrinsic averaging time τ_a. In Eq. (38), T_c is the integral time scale of the turbulent concentration fluctuations defined as

$$T_c = \int_0^\infty R(\tau)\, d\tau, \tag{39}$$

where $R(\tau)$ is the autocorrelation function of the concentration fluctuations (τ is the correlation lag time).

A parameterization of the integral scale for concentration fluctuations has been suggested by Sykes [33]. The effects of time-averaging imposed by a detector can be accounted for by using a model to predict the unaveraged concentration variance $\overline{c'^2}_p$ (or, equivalently, the unaveraged mean-square concentration $\overline{c^2}_p$), and then using Eq. (38) to compute the concentration variance, $\overline{c'^2}_p|_{\tau_a}$, appropriate for the averaging time τ_a imposed by the detector. It is this value of the predicted concentration variance (or, equivalently, mean-square concentration) that should be used in Eq. (32) in the specification of $f(\overline{c^2}|S)$.

It should be noted that the averaging imposed by a slower response detector (e.g., with response time greater than a few seconds) depends critically on the concentration integral time scale T_c. For example, at short range in unstable conditions, the highest concentrations have very short durations (and, hence, small integral time scales), and consequently the time averaging imposed by a detector may be significant in this case because concentration fluctuations shorter than about 1 s are averaged in most chemical agent detectors (e.g., CAM and AP4C which have typical averaging times of 5–10 s). However, under stable conditions, the peak concentrations have much longer durations and are also higher relative to the mean concentration. Under these conditions, the integral time scales of concentration are longer and, as a consequence, the concentration fluctuations would not be smoothed out by a chemical agent detector to the same extent. The same situation applies to dispersion in a built-up (urban) environment, where vigorous mixing of plume elements in canopy turbulence results in a dramatic increase in the integral time and length scales here [17]. More specifically, the enhanced and rapid mixing of plume material in a built-up area merges small-scale plume concentration structures, leading to a reduction in the frequency and number of low-amplitude events and high amplitude bursts relative to that in a comparable open-terrain plume, the net effect of which is to increase the concentration fluctuation integral time scale T_c.

7 Conclusions

This report examines the form of the concentration PDF for plumes dispersing in various obstacle arrays (built-up environment). The form of the concentration PDF was studied by examining the relationships between various normalized higher-order concentration moments using a large and comprehensive data set obtained from a series of measurements of plume dispersion in a number of obstacle arrays made in a boundary-layer water channel using high-resolution laser-induced fluorescence. For the present study, we extracted a large number of concentration time series from a number of different experiments involving various obstacle arrays (e.g., various arrays of cubical and non-cubical obstacles in aligned and staggered arrangements with uniform, random, and alternating heights).

The key conclusions revealed by this analysis can be summarized as follows. A remarkably robust feature of all the concentration data was the observed collapse of the third- and fourth-order normalized concentration moments on the second-order normalized concen-

tration moment and of the observed (S, K) collapse to a series of "universal" curves. The collapse of the various concentration moments here was exactly the same as that observed in the CONFLUX concentration data for open-terrain plumes. This remarkable collapse suggests that the concentration PDF of plumes dispersing in either a built-up or open-terrain environment can be described adequately by at most two parameters (namely, a location parameter which can be chosen to be the mean concentration and a scale parameter which can be chosen to be the root-mean-square concentration or, equivalently, the concentration standard deviation). Finally, the observed relationships between the various higher-order normalized concentration moments were found to be adequately modeled (predicted) using either a clipped-gamma distribution or the simpler intermittent exponential distribution (which is a special case of the clipped-gamma distribution). However, the general shape of the observed concentration probability distribution is well modeled using the clipped-gamma distribution, but the intermittent exponential distribution provides a rather poor conformance with the observed concentration. Indeed, the clipped-gamma distribution captures correctly the form of both the lower and upper tails of the measured concentration probability distribution for array plumes.

The scientific case for using probabilistic/statistical methods to assess the consequences of a toxic release, rather than traditional deterministic methods, is overwhelming. In this paper, the implication of the form of the concentration PDF, for the formulation of a probabilistic model for the response of a chemical agent detector, is investigated in the context of the source reconstruction problem. To this purpose, the likelihood function of a chemical agent detector (e.g., CAM, AP4C), which only reports short time-averaged concentration levels discretized on an N_b-level bar scale, has been derived. The close connection between the likelihood function and the concentration PDF has been investigated in detail.

The likelihood function, which characterises the likelihood that a chemical agent detector will give a certain bar level reading for a hazardous gas release from a given source distribution S, was derived. The derivation explicitly accounts for (1) model/input uncertainties in prediction of C required in the definition of the concentration PDF; (2) model/input uncertainties in prediction of $\overline{c^2}$ required in the definition of the concentration PDF; (3) measurement noise in the detector; and, (4) time-averaging imposed by the finite response of the detector. This likelihood function can be used directly in Bayesian source inversion methodologies [27] that have been developed to determine unknown source characteristics (e.g., location, source strength, time of release, etc.) when given a finite number of noisy concentration measurements made by an array of detectors.

References

[1] ten Berge, W. F., Zwart, A., and Appelman, L. M. (1986), Concentration-time mortality response relationships of irritant and systemically acting vapours and gases, *Journal of Hazardous Materials*, 13, 301–309.

[2] Yee, E. (1996), A nonlinear dose-response model with an application to the reconstruction of the human mortality response surface from acute inhalation toxicity with sarin, (Suffield Memorandum No. 1476) Defence Research Establishment Suffield.

[3] Birch, A. D., Brown, D., Dodson, M., and Thomas, J. R. (1978), The turbulent concentration field of a methane jet, *Journal of Fluid Mechanics*, 88, 431–449.

[4] Borghi, R. (1988), Turbulent combustion modeling, *Progress in Energy and Combustion Science*, 14, 245–292.

[5] Chatwin, P. C. (1982), The use of statistics in describing and predicting the effects of dispersing gas clouds, *Journal of Hazardous Materials*, 6, 213–230.

[6] Csanady, G. T. (1973), *Turbulent Diffusion in the Environment*, D. Reidel, Dordrecht, the Netherlands.

[7] Jones, C. D. (1983), On the structure of instantaneous plumes in the atmosphere, *Journal of Hazardous Materials*, 7, 87–112.

[8] Barry, P. J. (1975), Stochastic properties of atmospheric diffusivity, (AECL-5012) Atomic Energy of Canada Ltd, Chalk River, Ontario.

[9] Hanna, S. R. (1986), The exponential probability density function and concentration fluctuations in smoke plumes, *Boundary-Layer Meteorology*, 37, 89–106.

[10] Lewellen, W. S. and Sykes, R. I. (1986), Analysis of concentration fluctuations from lidar observations of atmospheric plumes, *Journal of Climate and Applied Meteorology*, 25, 1145–1154.

[11] Sawford, B. L. (1987), Conditional concentration statistics for surface plumes in the atmospheric boundary layer, *Boundary-Layer Meteorology*, 38, 209–223.

[12] Mylne, K. R. and Mason, P. J. (1991), Concentration fluctuation measurements in a dispersing plume at a range of up to 1000 m, *Quarterly Journal of the Royal Meteorology Society*, 117, 177–206.

[13] Yee, E., Wilson, D. J., and Zelt, B. W. (1993), Probability distributions of concentration fluctuations of a weakly diffusive passive plume in a turbulent boundary layer, *Boundary-Layer Meteorology*, 64, 321–354.

[14] Yee, E. and Chan, R. (1997), A simple model for the probability density function of concentration fluctuations in atmospheric plumes, *Atmospheric Environment*, 31, 991–1002.

[15] Yee, E., Chan, R., Kosteniuk, P. R., Chandler, G. M., Biltoft, C. A., and Bowers, J. F. (1994), Experimental measurements of concentration fluctuations and scales in a dispersing plume in the atmospheric surface layer obtained using a very fast-response concentration detector, *Journal of Applied Meteorology*, 33, 996–1016.

[16] Yee, E., Chan, R., Kosteniuk, P. R., Chandler, G. M., Biltoft, C. A., and Bowers, J. F. (1995), The vertical structure of concentration fluctuation statistics in plumes dispersing in the atmospheric surface layer, *Boundary-Layer Meteorology*, 76, 41–67.

[17] Yee, E. and Biltoft, C. A. (2004), Concentration fluctuation measurements in a plume dispersing through a regular array of obstacles, *Boundary-Layer Meteorology*, 111, 363–415.

[18] Gailis, R. and Hill, A. (2006), A wind-tunnel simulation of plume dispersion within a large array of obstacles, *Boundary-Layer Meteorology*, 119, 289–338.

[19] Yee, E., Gailis, R. M., Hill, A., Hilderman, T., and Kiel, D. (2006), Comparison of wind-tunnel and water-channel simulations of plume dispersion through a large array of obstacles with a scaled field experiment, *Boundary-Layer Meteorology*, 121, 389–432.

[20] Klein, P., Leitl, B., Schatzmann, M., and Young, D. (2008), Concentration fluctuations in a downtown urban area – analysis of concentration data from the Joint Urban 2003 full-scale and wind tunnel measurements, In *Proceedings of 15th Joint Conference on the Applications of Air Pollution Meteorology with the A&WMA*, New Orleans, LA. Paper AIRPOL 6.2.

[21] Sykes, R. I., Lewellen, W. S., and Parker, S. F. (1986), A Gaussian plume model of atmospheric dispersion based on second-order closure, *Journal of Climate and Applied Meteorology*, 25, 322–331.

[22] Hilderman, T. and Chong, R. (2007), A laboratory study of momentum and passive scalar transport and diffusion within and above a model urban canopy, (DRDC Suffield CR 2008-025) Defence R&D Canada – Suffield.

[23] Davidson, M. J., Mylne, K. R., Jones, C. D., Phillips, J. C., Perkins, R. J., Fung, J. C. H., and Hunt, J. C. R. (1995), Plume dispersion through large groups of obstacles—a field investigation, *Atmospheric Environment*, 29, 3245–3256.

[24] Macdonald, R. W., Griffiths, R. F., and Hall, D. J. (1998), A comparison of results from scaled field and wind tunnel modelling of dispersion in arrays of obstacles, *Atmospheric Environment*, 32, 3845–3862.

[25] Yee, E., Lien, F.-S., Keats, A., Hseih, K.J., and D'Amours, R. (2006), Validation of Bayesian inference for emission source distribution using the Joint Urban 2003 and European Tracer Experiments, In *Fourth International Symposium on Computational Wind Engineering (CWE2006)*. Yokohama, Japan, 4pp.

[26] Keats, A., Yee, E., and Lien, F.-S. (2007), Bayesian inference for source determination with applications to a complex urban environment, *Atmospheric Environment*, 41, 465–479.

[27] Yee, E. (2007), Bayesian probabilistic approach for inverse source determination from limited and noisy chemical or biological sensor concentration measurements, In Fountain III, Augustus W., (Ed.), *Proceedings of SPIE, Chemical and Biological Sensing VIII*, Vol. 6554, 65540W, doi:10.1117/12.721630. 12 pp.

[28] Jaynes, E. T. (2003), *Probability Theory: The Logic of Science*, Cambridge University Press, Cambridge, UK.

[29] Yee, E., Chan, R., Kosteniuk, P. R., Chandler, G. M., Biltoft, C. A., and Bowers, J. F. (1994), Incorporation of internal fluctuations in a meandering plume model of concentration fluctuations, *Boundary-Layer Meteorology*, 67, 11–39.

[30] Yee, E. and Wilson, D. J. (2000), A comparison of the detailed structure in dispersing tracer plumes measured in grid-generated turbulence with a meandering plume model incorporating internal fluctuations, *Boundary-Layer Meteorology*, 94, 253–296.

[31] Sykes, R. I., Lewellen, W. S., and Parker, S. F. (1984), A turbulent-transport model of concentration fluctuations and fluxes, *Journal of Fluid Mechanics*, 139, 193–218.

[32] Hanna, S. R. (1987), The effect of line averaging on concentration flucutations, *Boundary-Layer Meteorology*, 40, 329–338.

[33] Sykes, R. I. (1984), The variance in time-averaged samples from an intemittent plume, *Atmospheric Environment*, 18, 121–123.

This page intentionally left blank.

Distribution list

DRDC Suffield TR 2008-077

Internal distribution

1 Author

1 H/HPS

2 Library (1 Hard/1 CD)

1 DG

1 DDG

1 SMO

1 Chf Sci

Total internal copies: 8

External distribution

DRDKIM

1 DRDKIM Report Collection (CD only)

DRDC

1 DSTHP

NDHQ

1 DJCP 5-7

1 J2 Sci Tech

2 Director General Health Services, Canadian Forces Medical Group Headquarters, R&D Command Group Coordinator, 118 1745 Alta Vista Drive, Ottawa, ON K1A 0K6

Other Canadian Forces

1 CFNBCS

1 RMC
Attn: Clarinda Olsen
Massey Library
Royal Military College
P.O. Box 17000, Station Forces
Kingston, ON K7K 7B4

United States

1 **CBR MOU**
OSA (CBD&CDP)
Attn: Dr. Robert Cohn
3050 Defense Pentagon
Room 3C257
Washington, DC 20301-3050
USA

1 **TTCP**
Defence Threat Reduction Agency
Attn: Dr. Sal Bosco
8725 John J Kingman Rd, Stop 6201
Ft Belvoir, VA 22060-6201
USA

United Kingdom

1 **CBR MOU**
Dr. Hon Huggins
Defence Science and Technology Laboratory
Bldg 231, Rm 25
Porton Down
Salisbury SP4 0JQ
United Kingdom

1 **TTCP**
Dr. Rick Hall
Defence Science and Technology Laboratory
Bldg 106
Porton Down
Salisbury SP2 7AD
United Kingdom

Australia

1 **CBR MOU**
Dr. Peter Gray
Human Protection and Performance Division
Defence Science and Technology Organization
506 Lorimer St
Fisherman's Bend
Victoria 3207
Australia

1 **TTCP**
Dr. Simon Oldfield

506 Lorimer Street
Fisherman's Bend
Victoria 3207
Australia

New Zealand

1 **TTCP**
Dr. Patricia Shaw
Defence Technology Agency (DTA)
Private Bag 32901
Devonport
Auckland
New Zealand

Total external copies: 15

Total copies: 23

This page intentionally left blank.

DOCUMENT CONTROL DATA

(Security classification of title, body of abstract and indexing annotation must be entered when document is classified)

1. ORIGINATOR (The name and address of the organization preparing the document. Organizations for whom the document was prepared, e.g. Centre sponsoring a contractor's report, or tasking agency, are entered in section 8.)

   Defence R&D Canada – Suffield
   Box 4000, Station Main, Medicine Hat, Alberta,
   Canada T1A 8K6

2. SECURITY CLASSIFICATION (Overall security classification of the document including special warning terms if applicable.)

   UNCLASSIFIED

3. TITLE (The complete document title as indicated on the title page. Its classification should be indicated by the appropriate abbreviation (S, C or U) in parentheses after the title.)

   The Concentration Probability Density Function With Implications for Probabilistic Modeling of Chemical Warfare Agent Detector Responses for Source Reconstruction

4. AUTHORS (Last name, followed by initials – ranks, titles, etc. not to be used.)

   Yee, E.

5. DATE OF PUBLICATION (Month and year of publication of document.)

   May 2008

6a. NO. OF PAGES (Total containing information. Include Annexes, Appendices, etc.)

   60

6b. NO. OF REFS (Total cited in document.)

   33

7. DESCRIPTIVE NOTES (The category of the document, e.g. technical report, technical note or memorandum. If appropriate, enter the type of report, e.g. interim, progress, summary, annual or final. Give the inclusive dates when a specific reporting period is covered.)

   Technical Report

8. SPONSORING ACTIVITY (The name of the department project office or laboratory sponsoring the research and development – include address.)

   Defence R&D Canada – Suffield
   Box 4000, Station Main, Medicine Hat, Alberta, Canada T1A 8K6

9a. PROJECT NO. (The applicable research and development project number under which the document was written. Please specify whether project or grant.)

   16QD40

9b. GRANT OR CONTRACT NO. (If appropriate, the applicable number under which the document was written.)

10a. ORIGINATOR'S DOCUMENT NUMBER (The official document number by which the document is identified by the originating activity. This number must be unique to this document.)

   DRDC Suffield TR 2008-077

10b. OTHER DOCUMENT NO(s). (Any other numbers which may be assigned this document either by the originator or by the sponsor.)

11. DOCUMENT AVAILABILITY (Any limitations on further dissemination of the document, other than those imposed by security classification.)

   (X) Unlimited distribution
   ( ) Defence departments and defence contractors; further distribution only as approved
   ( ) Defence departments and Canadian defence contractors; further distribution only as approved
   ( ) Government departments and agencies; further distribution only as approved
   ( ) Defence departments; further distribution only as approved
   ( ) Other (please specify):

12. DOCUMENT ANNOUNCEMENT (Any limitation to the bibliographic announcement of this document. This will normally correspond to the Document Availability (11). However, where further distribution (beyond the audience specified in (11)) is possible, a wider announcement audience may be selected.)

   Unlimited

13. ABSTRACT (A brief and factual summary of the document. It may also appear elsewhere in the body of the document itself. It is highly desirable that the abstract of classified documents be unclassified. Each paragraph of the abstract shall begin with an indication of the security classification of the information in the paragraph (unless the document itself is unclassified) represented as (S), (C), (R), or (U). It is not necessary to include here abstracts in both official languages unless the text is bilingual.)

The relationships between various normalized higher-order concentration moments have been investigated using a large data set of concentration fluctuations obtained in a boundary-layer water channel with high-resolution laser-induced fluorescence. This data set corresponds to a series of comprehensive measurements of plume dispersion in a number of obstacle arrays (e.g., various arrays of cubical and non-cubical obstacles in aligned and staggered arrangements with uniform and random heights). A remarkably robust feature of all the concentration data was the observed collapse, of the third- and fourth-order normalized concentration moments on the second-order normalized concentration moment and of the concentration kurtosis on the concentration skewness, to a series of "universal" curves. These "universal" curves were identical to those observed previously for open-terrain plumes, and are well modeled using either a clipped-gamma probability density function (PDF) or the simpler intermittent exponential PDF for the concentration. A comparison of the shape of the model probability distributions to the measured concentration data at various plume locations showed that the clipped-gamma distribution provided a good representation for the general distribution shape, whereas the simpler intermittent exponential distribution yielded a poor conformance to the measured concentration probability distribution (in spite of the fact that both of the model distributions gave a good representation for the first four concentration moments). The implication of the form of the concentration PDF, for the formulation of a probabilistic model for the response of a chemical agent detector, is investigated in the context of the source reconstruction problem.

14. KEYWORDS, DESCRIPTORS or IDENTIFIERS (Technically meaningful terms or short phrases that characterize a document and could be helpful in cataloguing the document. They should be selected so that no security classification is required. Identifiers, such as equipment model designation, trade name, military project code name, geographic location may also be included. If possible keywords should be selected from a published thesaurus. e.g. Thesaurus of Engineering and Scientific Terms (TEST) and that thesaurus identified. If it is not possible to select indexing terms which are Unclassified, the classification of each should be indicated as with the title.)

concentration fluctuations
concentration moments
obstacle arrays
concentration probability density function
chemical sensor response modeling

Defence R&D Canada

Canada's Leader in Defence
and National Security
Science and Technology

R & D pour la défense Canada

Chef de file au Canada en matière
de science et de technologie pour
la défense et la sécurité nationale

www.drdc-rddc.gc.ca